Deeply subducted continental fragments: I. Fracturing, dissolution-precipitation and diffusion processes recorded by garnet textures of the central Sesia Zone (Western Italian Alps)

Francesco Giuntoli[1], Pierre Lanari[1], Martin Engi[1]

[1]Institute of Geological Sciences, University of Bern, Baltzerstrasse 1+3, 3012 CH-Bern

5   *Correspondence to*: Francesco Giuntoli (francesco.giuntoli@plymouth.ac.uk)

Abstract. Complex zoning in garnet from micaschists of the Sesia Zone (Western Italian Alps) preserves evidence of two orogenic cycles and provides detailed insights into resorption, growth and diffusion processes induced by fluid pulses at high pressure. Data on local textures and mineral chemistry are combined with data derived from thermodynamic modelling to

10   understand and quantify these processes. Garnet shows low-Ca porphyroclastic cores that are stable at (Permian) granulite facies conditions. In one sample, the first garnet rim that surrounds the pre-Alpine granulite facies core indicates that pre-Alpine amphibolite facies metamorphism followed the granulite facies event. The cores show lobate edges and preserve inner fractures, which are sealed by high pressure Alpine garnet. This observation suggests that during the first stages of subduction, before hydration of these high temperature rocks, brittle failure of the garnet occurred, implying high strain

15   rates. Several Alpine rims show different textures indicative of interaction with hydrous fluid: (a) resorption-dominated textures produced lobate edges, at the expense of the outer part of the granulite core; (b) peninsulas and atoll garnets are produced by replacement reactions; (c) spatially limited resorption and enhanced transport of elements due the fluid phase is evident along brittle fractures and their immediate proximity. Thermodynamic modelling shows that all of these Alpine rims formed at eclogite facies conditions.

20   Structurally controlled samples allow these fluid-garnet interaction phenomena to be traced across a portion of the Sesia Zone, with decreasing in fluid-garnet interaction toward external areas (NW). Replacement of the Permian HT assemblages by hydrate-rich Alpine assemblages can reach nearly 100%. However, no clear relationship is visible between deformation structures and fluids that triggered eclogite facies metamorphism; suggesting disperse fluid flow.

1 Introduction

25   Unravelling the metamorphic and deformational history in polyorogenic complexes is challenging because relics from previous stages are partially or completely overprinted during the subsequent stages. Garnet is a robust and common metamorphic mineral commonly used to decipher these processes. It is stable over a wide range of P-T conditions and rock types (e.g. Spear et al., 1984;O'Brien, 1997) and the relatively slow intracrystalline diffusion at T<650°C allows growth zones to be preserved (e.g. Yardley, 1977;Spear, 1991;Carlson and Gordon, 2004;Caddick et al., 2010;Ague and Carlson,

2013). Below 700°C, garnet of a few hundred micrometres radius can retain compositional zoning for several tens of million years (Florence and Spear, 1991;Caddick et al., 2010). However, various processes may alter the garnet zoning record, notably intragranular diffusion or replacement reactions. Diffusion length depends on temperature, time, and composition, being generally faster for Fe2+, Mg and Mn than for Ca (Carlson, 2006). Replacement of garnet may partially or completely

5   obliterate garnet growth zones due to dissolution and reprecipitation processes (Putnis, 2002, 2009;Putnis and John, 2010;Ague and Axler, 2016). Relics will show resorption features, e.g. lobate or peninsular structures within a garnet growth zone, and sharp transitions in composition are observed (e.g. Cruz, 2011). If the entire centre of a garnet is replaced by other minerals, typical atoll garnet may form (Atherton and Edmunds, 1966;Cooper, 1972;Smellie, 1974;Homam, 2003;Cheng et al., 2007;Faryad et al., 2010;Cruz, 2011;Ortolano et al., 2014). Dissolution of garnet is thought to be linked to the presence

10   of a (reactive) fluid and may be followed by precipitation of new garnet with a different composition (Hames and Menard, 1993;Compagnoni and Hirajima, 2001;Cheng et al., 2007;Faryad et al., 2010;Wassmann and Stöckhert, 2013;Ortolano et al., 2014;Ague and Axler, 2016).

Reconstructing the polyorogenic history stored in garnet requires an understanding of both texture and compositional zoning, which provide insights about the mechanisms of reactions involving garnet. To investigate the problem, we combined high-

15   resolution electron probe compositional mapping with data derived from forward thermodynamic modelling, that accounted for fractional crystallisation and garnet resorption (Lanari et al., 2017). This approach was applied to several samples collected from the Internal Complex (as defined in Giuntoli and Engi, 2016) of the Sesia Zone, where garnet retains information from two very different orogenic cycles: Permian high-temperature and Alpine high-pressure. These polymetamorphic pre-Alpine garnets have been recognized since the works of Martinotti (1970), Compagnoni (1977), Zucali

20   et al. (2002), and Robyr et al. (2014). This type of garnet shows coarse and clear pre-Alpine porphyroclasts, generally mantled by a rim of Alpine garnet with a dusty appearance due to inclusions, which is also present as smaller crystals. During greenschist-facies Alpine retrogression, garnet crystals were partially retrogressed into chlorite, especially along crystal edges and fractures.

These garnets have been interpreted in two different ways by previous authors and we propose a third alternative in this

25   paper. Konrad-Schmolke et al. (2006) studied similar complex garnet zoning patterns, suggesting that they do not reflect two orogenic cycles, but are related to different water contents of the protoliths during Alpine HP subduction. In water-saturated rocks garnet would then display a typical prograde zoning; whereas in water-undersaturated rocks garnet would produce more complex zoning, including an abrupt compositional change from the core to the rim.

Robyr et al. (2014) interpreted the texture of these garnets as matrix-dependent: Garnet forms mushroom- and atoll-shaped

30   crystals in quartz-rich layers, but large idioblastic crystals in mica-rich layers. Four growth zones were identified, the first three of which modelled as stable during prograde pre-Alpine Barrovian metamorphism from 500°C and 0.6 GPa to 600°C and 0.9 GPa, whilst the fourth zone was modelled as stable at 550°C and 1.7-2.2 GPa, hence it is Alpine in age. Three processes have been inferred to control the formation of atoll garnet: simultaneous multiple nucleation and coalescence processes (e.g. Cooper, 1972;Spiess et al., 2001), rapid and short-term poikiloblastic growth (e.g. Atherton and Edmunds,

1966;Ushakova and Usova, 1990), and resorption plus re-crystallization of the garnet core (e.g. Smellie, 1974;Homam, 2003;Cheng et al., 2007). Robyr et al. (2014) proposed a fourth process that may produce atoll garnet textures: a change in the stoichiometry of the garnet-forming reaction, from small amounts of quartz being consumed during the pre-Alpine history to a situation with elevated solubility of quartz in the presence of high-pressure fluids.

5 In this study, we propose that repeated local resorption and growth of garnet produces complexly zoned garnet with lobate textures, peninsular features and, in the most extreme cases, formation of atoll garnet. Localized intragranular diffusion is observed only in the proximity of fractures that were probably acting as a main fluid pathway. We used microstructural analysis and compositional maps to analyse garnet resorption and replacement processes that we believe are related to the amount of fluid-rock interaction in a series of four samples collected 2 kilometres perpendicular to the main foliation and 5

10 kilometres along strike of the Internal Complex. Textural changes are related to processes of dissolution, growth and diffusion. Furthermore, quantitative pressure (P) and temperature (T) information of single garnet growth zones (data from Lanari et al., 2017; Giuntoli, 2016;Giuntoli et al., submitted) are discussed in relation with the microstructures.

2 Geological setting

15 The Alpine orogenic belt formed between the Cretaceous and the Oligocene as a result of the convergence of the European plate and the Adriatic plate (Dewey et al., 1989;Rosenbaum et al., 2002;Handy et al., 2010). The Sesia Zone is a major high-pressure continental unit located in the Italian Western Alps (Fig. 1a). It is thought to derive from the distal portion of the Adriatic passive margin that was involved in the Alpine subduction (Dal Piaz, 1999;Beltrando et al., 2014). The Sesia Zone is bounded to the west by blueschist to eclogite facies subunits derived from the Piemontese-Liguria Ocean (Bearth,

20 1967;Dal Piaz and Ernst, 1978;Martin et al., 1994;Cartwright and Barnicoat, 2002;Bucher et al., 2005;Groppo et al., 2009;Rebay et al., 2012;Negro et al., 2013) and to the east by the Insubric Line. This dextral brittle fault separates the Sesia Zone from the Southern Alps, which show but a weak Alpine imprint at sub-greenschist facies (Bertolani, 1959;Zingg, 1983).

In the Aosta Valley (Fig. 1b) the Sesia Zone comprises two main complexes, i.e. the Internal and External Complexes (IC

25 and EC hereafter; Giuntoli and Engi, 2016) separated by a greenschist facies shear zone. The EC comprises three epidote blueschist facies sheets of orthogneiss, with only minor paragneiss and metasediments, which are separated by lenses and bands, classically named Seconda Zona Diorito-Kinzigitica (2DK; Artini and Melzi, 1900;Dal Piaz et al., 1971;Compagnoni et al., 1977); these retain a pre-Alpine high temperature imprint and only local evidence of the Alpine HP-history. The IC consists of several eclogitic units, each 0.5–3 km thick, separated by presumed monometamorphic (Mesozoic) meta-

30 sediments (Venturini et al., 1994;Regis et al., 2014;Giuntoli and Engi, 2016). This complex is characterized by interlayered micaschist, eclogite, ortho- and paragneiss, with a minor portion of pre-Alpine marbles and Mesozoic metasedimentary bands (e.g. Compagnoni, 1977;Castelli, 1991). The IC experienced eclogite facies conditions during Alpine metamorphism,

with maximum recorded pressure of 2 GPa and temperature of 650-670 °C, between 85 and 55 Ma (Compagnoni, 1977;Konrad-Schmolke et al., 2011;Rubatto et al., 2011;Regis et al., 2014). Minor and local retrograde blueschist and greenschist facies overprint is present, especially close to tectonic contacts (Babist et al., 2006;Giuntoli and Engi, 2016). The IC preserves rare relics of pre-Alpine (Permian) granulite (0.6-0.9GPa, ~850°C) and retrograde amphibolite conditions (0.5-0.3 GPa, 570-670°C; Lardeaux and Spalla, 1991;Rebay and Spalla, 2001;Zucali et al., 2002).

3 Analytical methods

Thin sections were studied by optical microscopy to characterize the structural and metamorphic relations among the main mineral phases. Backscattered electron (BSE) images were obtained using a Zeiss EVO50 scanning electron microscope of the Institute of Geological Sciences, University of Bern, using an accelerating voltage from 15 to 25 keV, a beam current of 500 pA and a working distance of 10 mm.

Electron probe micro-analyses (EPMA) were performed using a JEOL JXA-8200 superprobe at the Institute of Geological Sciences, University of Bern. For compositional mapping, the procedure of Lanari et al. (2013) was used. Spot analyses were measured for each mineral phase present in the area of the maps before the latter were acquired. The investigated areas were mapped in wavelength-dispersive mode (WDS), with point analyses serving as internal standard. For point analyses, the analytical conditions were 15 KeV accelerating voltage, 20 nA specimen current, 40 s dwell times (including 2×10 s of background measurement) and ~1 μm beam diameter. Nine oxide compositions were analysed, using synthetic and natural standards: wollastonite/almandine (SiO_2), almandine (Al_2O_3), anorthite (CaO), almandine (FeO), spinel (MgO), orthoclase (K_2O), albite (Na_2O), ilmenite (TiO_2), and tephroite (MnO). For X-ray maps, analytical conditions were 15 KeV accelerating voltage, 100 nA specimen current and dwell times of 150-250 ms. Nine elements (Si, Ti, Al, Fe, Mn, Mg, Na, Ca and K) were measured at the specific wavelength in two passes. Intensity maps were standardized using spot analyses as internal standard. X-ray maps were classified and standardized using XMAPTOOLS 2.2.1 (Lanari et al., 2014). Structural formulae and end-member proportion maps were generated using the external functions provided in XMAPTOOLS (Lanari et al., 2014). Major element compositions were analysed by X-ray fluorescence (XRF) spectrometry at the University of Lausanne (Switzerland). Representative amounts of samples were crushed and then pulverized inside a tungsten carbide mill. The powder was dried for two hours at 105°C. Loss of ignition was then determined by weight difference after heating to 1050°C for 3 hours.

4 Petrography

The samples investigated are pelitic micaschists of the IC of the Sesia Zone displaying pale orange to greyish weathering surfaces. Grain sizes range from sub-millimetric to a few centimetres (detailed description in the Supplement), with garnet in all samples showing either a single or bimodal size range. In this paper the term large grains refer to garnet several

millimetres in diameter, small grains if are 50-200 μm in diameter. In plane-polarized transmitted light large garnet shows a clear core surrounded by a first rim that is dark due to finely dispersed inclusions, mostly of rutile needles (5-20 μm; Fig. 2). Adjacent to this cloudy rim, some garnet grains show a clear outermost rim. The same core-rim structure is visible in BSE images, in which the core is brighter than the rims (e.g. Fig. 5a). In detail, garnet observed in each sample shows slightly

5   different textures and compositions; petrographic and microstructural characteristics are summarized below and in Table 1. The four samples were collected from internal areas (South East - FG1315 and FG12157) to external area (North West- FG1249 and FG1347) of the IC (Fig. 1b). Major element compositions for the samples are shown in the Supplement Table S1. FG1315 is a garnet white mica schist with a foliation marked by phengite, paragonite and allanite (Fig. S1). Garnet displays two different micro-textures: (a) large crystals preserving a porphyroclastic core plus overgrowth zones, and (b)

10   atoll garnet a few hundred microns in size. Where the garnet core is preserved, it is optically clear and shows inclusions of rutile containing rare ilmenite relics. The first garnet rim appears cloudy due to finely dispersed rutile inclusions, the outer rim is clear with few and coarser rutile inclusions (Fig. S5b). Both rims contain abundant quartz inclusions. Atoll garnet is optically clear; its core is now mainly composed of quartz and sparse phengite. Brittle fractures in both garnet types are lined by minor late chlorite.

15   FG12157 is a glaucophane garnet micaschist. Its foliation is deformed by open folds and marked by phengite, glaucophane, and allanite (Fig. S2). Garnet is present as large grains with a clear core with several quartz inclusions at the periphery. The first garnet rim (Rim1) is dark, due to fine sagenitic rutile inclusions, locally as needles with a 120° intersection that may mark dissolved Ti-rich biotite. The second garnet rim (Rim2) is more clear (Fig. 2). Glaucophane and phengite locally occur within Rim1 or between Rim1 and Rim2. Apatite inclusions are presents in the core and both rims.

20   FG1249 is a rutile garnet micaschist with phengite, paragonite, allanite, and rutile defining an intense foliation that wraps around garnet of several millimetres size (Fig. S3). Garnet shows an optically clear core and a dark rim due to finely dispersed rutile (μm size) and paragonite inclusions. Coarser rutile (up to 100 μm) is included in the core as well as are phengite and apatite core; paragonite and quartz are concentrated at the core-rim transition. Some late chlorite fractures dissect entire garnet grains.

25   FG1347 is a chloritoid garnet micaschist with a strong foliation marked by phengite, chloritoid, paragonite, and rutile (Fig. S4). Garnet is several millimetres in size, with a clear core and a dark rim full of fine rutile inclusions, as in the other samples. Quartz inclusions are abundant in the rim (Fig. S6b).

5 Results

5.1 Compositional zoning in garnet

30   High-resolution X-ray maps are most helpful to study garnet microtextures, because element distributions are visible showing growth patterns. The complex geometry of end-member proportion maps reveals several zones of distinct composition (Fig. 2-3) surrounding the garnet core, which are visible neither by optical microscopy nor in backscatter

electron pictures. While some geometric variability is evident among individual grains and from one sample to another, certain prominent features are observed in most of them. Maps of grossular fraction (X_{Grs}, Fig. 3) provide the clearest distinction of the growth zones and are most suitable to identify similarities among all the samples. Generally, maps of the almandine and pyrope fractions provide patterns similar to grossular (except in one sample, FG1249). The common feature evident in X_{Grs} maps of all the samples is a core poor in Ca, containing fractures sealed by a more calcic garnet. The core is surrounded by several rims, all of them higher in X_{Grs} (Fig. 3), but subtle differences exist between the rims of each specimen, as discussed in the following sections.

Two types of fractures are visible: millimeter-long fractures within which chlorite crystallized (black colour in Figs 2c, 3), and micrometer-size cracks visible only in compositional maps, forming a fracture network in garnet cores, which has been sealed by garnet richer in grossular (Figs. 2, 3). Average compositions of garnet growth zones are reported in Table 2.

5.1.1 FG1315

The X_{Grs} map shows a porphyroclastic core of uniform composition ($Alm_{68}Prp_{27}Grs_4Sps_1$), with lobate edges and a dense network of micrometric fractures sealed by more calcic garnet ($Alm_{67}Prp_{23}Grs_9Sps_1$; Figs. 3a, S5). Rim1 surrounds the rounded relic core and is higher in grossular content ($Alm_{60}Prp_{20}Grs_{19}Sps_1$) that the core; Rim1 is thinner in the direction of the main foliation, peninsular growth of Rim1 extends into the core. Rim2 ($Alm_{64}Prp_{24}Grs_{11}Sps_1$) grew on both sides of Rim1 (internally and externally) and also yielded fine veins that dissected entirely Rim1 (as discussed in section 6.2). Rim2 also surrounds and thus extends the Rim1 peninsula inside the core. The outermost rim (Rim3) is lower in grossular ($Alm_{69}Prp_{24}Grs_6Sps_1$), it displays peninsular growths inside Rim1 and Rim2. Remarkably, Rim3 is thicker perpendicular to the main foliation.

Zoning patterns in atoll garnet (Fig. 4) are analogous, as are the grossular contents. The inner growth surfaces of Rim1 define negative garnet crystal forms, whereas Rim2 overgrowths are present on the outside growth surface only. Rim3 is the outermost growth zone with peninsulas at the expenses of the previous rims.

5.1.2 FG12157

Garnet cores are chemically zoned with domains showing high spessartine and pyrope contents but relatively low almandine fractions (Fig. 5; zoning profile of the garnet end-member in Fig. 2 of Lanari et al., 2017). The porphyroclastic core (average composition: $Alm_{69}Prp_{25}Grs_4Sps_2$) shows lobate edges and is fractured, but cracks are sealed by more calcic garnet ($Alm_{66}Prp_{21}Grs_{12}Sps_1$; Figs. 2b, 3b, 5c). Three overgrowth zones surround the core: Rim1 is higher in grossular ($Alm_{63}Prp_{20}Grs_{16}Sps_1$) than the core; Rim2 is higher yet ($Alm_{59}Prp_{17}Grs_{23}Sps_1$) and grew both internally and externally of Rim1. Rim3 is present just locally as the outermost rim ($Alm_{64}Prp_{20}Grs_{15}Sps_1$).

5.1.3 FG1249

A core and three rim generations are evident in the compositional maps (Fig. 6; zoning profile in Fig. 7). As in the other sample, the core is lowest in grossular ($Alm_{72}Prp_{18}Grs_5Sps_5$) and shows a fracture pattern, which was sealed by garnet with a higher grossular content ($Alm_{60}Prp_{18}Grs_{20}Sps_2$; Figs. 3c, 6c). Compared to the core, Rim1 is higher in grossular

5   ($Alm_{75}Prp_{15}Grs_9Sps_1$) and its outer edge is euhedral. Rim2 is higher in grossular than the previous growth zone ($Alm_{62}Prp_{20}Grs_{17}Sps_1$) and quite similar to the fracture fillings. It is variable in thickness, but present both at the core-Rim1 boundary and peripheral to Rim1. Rim3 is the outermost growth zone and highest in grossular ($Alm_{58}Prp_{18}Grs_{23}Sps_1$). Its thickness varies, giving the entire garnet a euhedral shape. Locally, Rim3 is present also at the core-Rim1 boundary (Fig. 7). This zoning pattern shows different features along the main fracture zones and around them: a sharp and strong decrease in

10   Alm and Sps and increase in Prp content is visible. Rim 1, 2 and 3 are also found in small garnet crystals (ø 0.1-0.5 mm) in which a core is not visible.

5.1.4 FG1347

The core is zoned with patchy areas high in X_{Sps} and X_{Alm} but low in X_{Prp} (Fig. S6). The X_{Grs} map (Fig. 3d) reveals a dense fracture pattern in the core ($Alm_{68}Prp_{27}Grs_3Sps_2$) sealed by more calcic garnet ($Alm_{68}Prp_{25}Grs_6Sps_1$). These fractures stop

15   immediately against Rim1, which is highest in grossular content ($Alm_{66}Prp_{22}Grs_{11}Sps_1$). Rim2 ($Alm_{67}Prp_{26}Grs_6Sps_1$) is strongly asymmetric: it is wider perpendicular to the main foliation, as are Rim3 ($Alm_{69}Prp_{26}Grs_4Sps_1$) and Rim4 ($Alm_{71}Prp_{25}Grs_3Sps_1$), suggesting syn-kinematic growth in a simple shear regime (involving rotation of garnet; e.g. Johnson 1993, Robyr et al. 2009). Additionally, clasts of Rim2, Rim3 and Rim4 are partly dismembered from the main garnet crystal, possibly due to deformation by the same mechanism.

20   **5.2 Results of thermodynamic modelling of garnet growth zones**

PT estimates obtained from the garnet growth zones are summarized here with the main purpose of distinguishing between pre-Alpine (HT) and Alpine (HP) growth periods. The complex textures and partial replacement of garnet inferred from these required the development of a novel approach of forward thermodynamic modelling tools; optimized P-T conditions of each growth zone presented below were obtained using the program GRTMOD (Lanari et al., 2017). It is initially based on

25   bulk rock compositions, but these are modified at each step to account for fractional crystallization and partial resorption. The full dataset used is available in Giuntoli (2016) and Giuntoli et al. (submitted). Figure 8 summarizes the composition of all the garnet growth zones in a ternary diagram (Alm, Prp, Grs) and the optimal P-T conditions determined for each growth zone. Notably, in each sample studied the crystals analysed in thin section all show the same chemical zoning pattern. Garnet cores in all modelled samples indicate growth at granulite facies conditions (Fig. 8); only in sample FG1249 the

30   garnet core shows an overgrowth (Rim1) that is considered pre-Alpine, since modelling indicates amphibolite facies conditions (Fig. 8). In the terrain sampled, i.e. the central Sesia Zone, HT conditions at low to intermediate pressures, i.e.

granulite and amphibolite facies are well established from the upper Paleozoic (Kunz et al., 2017), but have never been reported for the Alpine metamorphism, which is of eclogite facies grade. And indeed, all of the subsequent garnet rims in the samples studied have formed in the eclogite facies, hence in the Alpine cycle, as shown by HP mineral inclusions as phengite, glaucophane and rutile (see section 4; Figs. 4b, 5b, 6b, S5b, S6b) and our results of P-T modelling (Fig. 8).

5 Conditions found from one sample to the next show minor differences, indicating spatial and/or temporal gradients in the P-T conditions. These may not all have been captured in all samples at the exact same time of the evolution of the belt.

FG1315: The garnet core is predicted at ~0.8 GPa and 750 °C. The HP Alpine rims are modelled at ~1.5 GPa and 650°C, 1.9 GPa and 650°C, 1.8 GPa and 670°C respectively.

FG12157: Modelling indicates ~0.6 GPa and 900 °C for the core; Alpine Rim1 and Rim2 are predicted at ~1.6 GPa, 650°C

10 and ~1.4 GPa, 630°C, respectively.

FG1249: The pre-Alpine core is modelled at ~0.6 GPa and 730°C. Rim1 crystallized in pre-Alpine amphibolite facies conditions (~0.6 GPa and 620°C). Alpine Rim2 and Rim3 crystallized at ~1.6 GPa, 620°C and 1.5 GPa, 660°C, respectively.

FG1347: The pre-Alpine core is modelled stable at ~0.8 GPa and 770°C. The Alpine rims (1-3) are modelled stable between 1.7-2.0 GPa and 580-600°C.

15 **6 Discussion**

Garnet cores are modelled stable in granulite facies conditions; Rim1 of sample FG1249 suggests amphibolite facies conditions. In situ U-Pb dating of metamorphic growth rims in zircon from all the samples presented in this study gave lower Permian weighted mean ages (~295-280 Ma; Kunz et al., 2017). These data are in agreement with the late Permian retrograde metamorphism from granulite to amphibolite facies condition estimated by Lardeaux and Spalla (1991) and

20 Rebay and Spalla (2001). Except for Rim1 in FG1249, all the garnet rims modelled are found to be stable at eclogite facies conditions that are comparable to those previously determined for the central Sesia Zone (e.g. Konrad-Schmolke et al., 2006;Konrad-Schmolke and Halama, 2014;Regis et al., 2014;Rubatto et al., 2011;Lanari et al., 2017). In the following, the main textures recognized in garnet are discussed and related to specific processes.

6.1 Micrometre-size fracture network in garnet cores

25 A network of fractures is present in all of the pre-Alpine cores of the samples (Fig. 3). These fractures have a size from few microns to some tens of microns and an irregular shape with sharp edges and conjugate systems with 90 degrees interception. The fractures are not visible by optical or scanning electron microscopy, as they are sealed by a garnet similar in composition to the first HP Alpine generations. These small-scale fillings formed probably coevally with one of the first Alpine garnet rims, as they share a similar chemical composition.

30 In outer parts of the core fractures are less abundant, and the more calcic garnet fillings show sharp boundaries against the old garnet core composition. In central parts the core appears "cloudy", owing to the dense network of sealed cracks, so the

finely spaced veins of new garnet are more difficult to discriminate. Minor diffusional smoothing may also have occurred over a scale up to ten microns. Enhanced diffusion in the proximity of fractures has been reported from similar environments and related to fluid circulation (e.g. Erambert and Austrheim, 1993; see §6.3). In the present samples, the fracture network in garnet cores is best visible in the X_{Grs} maps, but is also evident in other X-ray maps, notably of Fe and Mg, but less of Mn

5   (except for FG1249), possibly because the concentration is too low to detect such a small variation in Mn. Grossular fraction has long been known to be strongly pressure-dependent Kretz, 1959, and pressure is the physical variable expected to vary particularly in a subduction setting. Moreover, among the divalent elements in garnet and up to fairly high temperature, Ca is least affected by diffusion (e.g. Carlson 2006), hence most likely to retain growth features.

The network of cracks reflects brittle deformation in garnet, which implies a small ductility contrast between garnet and the

10   matrix (e.g. Raimbourg et al., 2007) and high strain rates that may have been related to seismic failure (Austrheim et al., 1996; Austrheim et al., 2017; Angiboust et al., 2012). Since the mineral assemblages formed by Permian granulite facies metamorphism were mostly anhydrous prior to the HP Alpine (re)hydration (Engi et al., in preparation), the rheological contrast between garnet and its matrix is expected to have been small. As we show in the following, fractures in a rheologically strong mineral like garnet and their subsequent sealing thus provide a link from the Permian HT- to the

15   Cretaceous HP-conditions, more specifically related to the first stage of fluid influx (Fig. 9a). In other samples from the IC of the Sesia Zone, brittle behavior of garnet is manifested by trails and pods of garnet fragments (some hundred microns in size) that represent torn apart garnet porphyroclasts (Trepmann and Stöckhert, 2002). Such garnet clasts only partially recrystallized to form more idiomorphic crystals. We cannot rule out that some of the fractures developed in pre-Alpine time, notably in an extensional tectonic setting. This has been proposed for other localities Floess and Baumgartner, 2013, where

20   garnet breakdown occurred at LT and LP, involving a volume increase and hydration. However, in the present case, micrometer-wide fractures dissect pre-Alpine garnet, the coherence of these fractured grains is preserved. We found no chemical evidence of any LT- or LP-alteration predating the growth of Ca-enriched garnet, except for one sample (FG 1249, discussed below). All these observations indicate an Alpine origin for the fracture network and suggest that these were yielded by a new garnet generation before the fragments were dismembered by subsequent strain. Most probably the

25   formation of fractures and growth of garnet inside the fractures were closely related, and mineral compositions indicate that this occurred at HP conditions.

6.2 Resorption and growth: fluid-related textures

The studied samples record several stages of resorption with unequal portions of garnet being affected (Fig. 3). Sample FG1315 shows most extensive resorption, as judged by textures: lobate edges, peninsular structures, veins inside Rim1, and

30   formation of atoll garnet (Figs. 3b, 4, 9, S5). In particular, the vein network dissects Rim1, resorption is evident along these veins and on both sides of Rim1, followed by precipitation of Rim2. Note that Rim2 displays the same chemical composition in all of these domains. For this reason, we surmise that Rim1 and 2 are not a simple growth sequence, with the older generation in a more internal position and younger ones more externally. Instead, the older growth zone (Rim1) was partially

resorbed and replaced by a younger one (Rim2) that precipitated on both sides. This interpretation is also supported by numerous micrometre-size rutile inclusions in Rim1; these highlight paleo-porosity, an essential feature of the replacement processes (e.g. Putnis, 2015). Analogous zoning patterns are also evident in samples FG12157 and FG1249 Rim1 and 2, even though the vein network is less clearly visible in the compositional maps. Atoll garnet may form by several processes,

5   such as rapid poikiloblastic growth, multiple nucleation and coalescence processes, change in reaction stoichiometry, dissolution of the core that was rendered unstable (by changes P-T conditions), and precipitation of a new garnet stable in presence of fluid circulation (e.g. Faryad et al., 2010;Robyr et al., 2014;Ortolano et al., 2014). Based on all the evidence in sample FG1315, we conclude that atoll garnet formation was related to partial dissolution of the unstable HT-core under HP-conditions. Note that the effect of this process is grain size dependent, and the atoll garnet cores observed in this sample are

10   limited in size from 50 to a few hundred microns. Destabilization of these small garnets lead to complete replacement of the core, whereas large garnet cores (up to several mm in size) reflect partial resorption, showing lobate structures or peninsular features, but the entire core was not replaced (Fig. 9b). Detailed thermodynamic modelling (Lanari et al., 2017) predicts extensive resorption of garnet cores during the formation of Rim3. In FG1315, resorption textures are also visible in the Permian growth zone of zircon, as documented by Giuntoli (2016) and Giuntoli et al. (submitted). Resorption occurred at

15   several stages, as visible from the peninsulas in which garnet Rim1 crystallized and was successively enlarged by Rim2 and by Rim3 peninsulas at the expense of both Rim1 and Rim2. Figure 9b summarizes the growth / resorption chronology of garnet in this sample.

Resorption and growth textures in sample FG12157 are similar to those in FG1315, except that no atoll garnet was observed. However, a drastically different type of textural features was found in sample FG1249: Neither clear lobate structures nor

20   peninsulas indicate resorption, except for a narrow Rim2 that grew at the expense of garnet core and Rim1. The growth chronology of the sample FG1249 is summarized in Fig. 9a. In sample FG1347 resorption traces are limited close to the fracture network in the core, with minor resorption of Rim2 (Fig. 3d).

With one exception, all of the samples presented above also contain zircon and sparse monazite; these are only preserved as pre-Alpine (Permian) relics in the core of Alpine allanite. The exception is FG12157 where monazite is completely

25   pseudomorphed by allanite and apatite; (Kunz et al., 2017). Apart from garnet and these accessory relics, the main pre-Alpine HT assemblage has completely re-equilibrated at eclogite facies conditions. This is also evident from the volatile contents of these samples and their high percentages of hydrous minerals: LOI (loss-on-ignition) values range from 1.58% to 2.44% compared to values of 0.5-0.7 wt% for proposed equivalent rocks in the Ivrea Zone, i.e. pre-Alpine upper amphibolite to granulite facies samples lacking an Alpine facies overprint (Engi et al., in preparation). As detailed in that study, this

30   implies that the nominally dry pre-Alpine HT assemblages were replaced in response to disperse infiltration of hydrous fluid. This Alpine hydration process occurred in several pulses or stages (Fig. 9). Previous partial hydration is evident only in one sample (FG1249), in which a first rim formed during pre-Alpine retrogression from granulite to amphibolite facies conditions. In all other cases studied, the increase in bulk rock volatile contents happened during the Alpine HP-evolution,

when fluid was imported while the IC was in the subduction channel. This hydration is expected to have enhanced ductile deformation and metamorphic reaction rates (Austrheim, 1990;Austrheim et al., 1997).

6.3 Re-equilibration close to fluid pathways

As described in section 5.1.3, fractures in the pre-Alpine garnet cores are evident in X-ray maps made from sample FG1249,
5 and all garnet end member maps show that these are sealed by garnet of a composition ($Alm_{62}Prp_{18}Grs_{18}Sps_{2}$) similar to the first two Alpine rims (Rim2 and Rim3). Note that the core is chemically uniform, as expected in granulite facies garnet owing to fast diffusion at high temperature (e.g. Caddick et al., 2010). However, in an area some 500 μm wide (indicated by white arrows in Fig. 6), garnet is affected by fractures, and the $X_{Alm, Prp, Sps}$ maps show that it is compositionally different from the core, except for a few islands where original granulite facies garnet remains, and it displays an Alpine composition
10 (Figs. 6, 7). This feature is best seen in the Mn-map, which serves as a marker delimiting the original pre-Alpine garnet core with its high X_{Sps} values (0.05-0.06; Fig. 6f). Overprinted areas show a sharp decrease in X_{Sps}, down to values of 0.02. The X_{Grs} map (Fig. 6a) is drastically different, as garnet displays the same composition as pristine pre-Alpine generations (Grs5 and 9 for core and Rim1, respectively), except just a few microns away from the fractures.

This zoning pattern suggests that fractures provided fluid access, initiating a re-equilibration process that affected the
15 surrounding volume of garnet over a distance of several hundred microns. As minor fractures are visible branching from the major ones, we consider this area as a damaged zone in which re-equilibration of the garnet was enhanced along a network of micro-fractures and in their proximity, due to the increased area/volume ratio (Austrheim et al., 1996). Erambert and Austrheim (1993) reported similar vein patterns in pre-Caledonian granulite garnet of the Bergen Arcs (Western Norway), and they interpret these as fluid channels along which element mobility was enhanced. These studies concluded that re-
20 equilibration of granulite-facies garnet during Caledonian eclogite conditions occurred proportionally to the fracture density and fluid availability.

This re-equilibration process was evidently much more effective for Alm, Prp, and Sps than for Grs. We propose that diffusion of Ca ions through the damaged lattice of the original garnet was slower than of Fe^{2+}, Mg, and Mn. Conspicuously similar phenomena were observed by Erambert and Austrheim (1993). Their evidence is in line with what we discussed
25 above, i.e. that new garnet formed just along the fractures; in the neighbouring area strong overprinting of original garnet is observed for Prp, Alm and Sps but not for Grs. Raimbourg et al. (2007) advanced that intra- and inter-granular transport of Ca in garnet is inefficient compared to Fe^{2+} and Mg. Volume diffusion of divalent ions is slow in garnet at temperatures below 700 °C (Ganguly, 2010), but differences in interdiffusion between Ca, Mg, Fe, and Mn are notable (e.g. Carlson, 2006).
30 In the latest phases of this re-equilibration process, brittle fractures would have been sealed by the Alpine garnet visible along the fracture walls. This might have occurred in several stages, as can be inferred from the X_{Grs} map, where garnet sealing the fractures has the composition of Rim2 and Rim3 (Figs. 6, 7).

X_{Sps} can be used as a tracer of re-equilibration processes also in samples where the effect of such processes on garnet texture it is not as striking as for FG1249. This is the case in samples FG12157 and FG1347, in which high fracture density corresponds with low spessartine values (Figs. 5f, S6f). Furthermore, zoning found in the core of FG1347 for Alm, Prp and Sps is not evident in the X_{Grs} map, again indicating that re-equilibration in the proximity of the main fluid pathways was more effective for Fe^{2+}, Mg, and Mn than for Ca ions.

6.4 Hydration through the IC

The previous section used garnet textures linked to the main paragenesis and P-T modelling to show that the IC of the central Sesia Zone in the Aosta Valley underwent pre-Alpine granulite facies metamorphism with local amphibolite facies retrogression, followed by major Alpine hydration occurring at different stages of the eclogite facies evolution. In detail, garnet suggests a decrease in the amount of fluid-garnet interaction textures and related pervasive resorption features from internal areas (South East - FG1315 and FG12157) to external area (North West- FG1249 and FG1347) of the IC (Fig. 1b). Such a tendency is supported by field observation (Giuntoli and Engi, 2016), as the only mesoscopic boudin of pre-Alpine amphibolites found in the area of the IC studied (Compagnoni, 1977) is located close to sample FG1347. These amphibolites are only partially re-equilibrated in eclogite facies conditions, and they preserve pre-Alpine hornblende and plagioclase (Compagnoni, 1977;Gosso et al., 2010).

Hydration in internal areas (SE parts) of the IC started during early subduction metamorphism, as recorded by prograde lawsonite (Zucali and Spalla, 2011) and continued up to the highest P-T conditions recorded in the present samples. In external (NW) areas of the IC a second generation of lawsonite provides evidence of hydration occurring right after rocks reached their HP climax, when temperature decreased (Pognante, 1989). This stage was related to H_2O-rich (low XCO_2) fluids possibly along preferential channels, producing metasomatism, as reflected by local occurrences of lawsonite in high modal amounts (up to 60 vol.-%).

In the central Sesia Zone (mainly in an area south of the Aosta Valley, whereas our samples were taken north of it), Konrad-Schmolke et al. (2006) found evidence that micaschists similar to those reported here also were not fully hydrated prior to Alpine subduction. Based on P-T modelling, that study concluded that extensive influx of hydrous fluid would have been required for these rocks to remain water-saturated between 1.2 and 1.8 GPa. This is similar to our results, but Konrad-Schmolke et al. (2011) invoked open-system pervasive fluid flow in the Tallormo Shear Zone and concluded that hydration occurred at retrograde blueschist conditions, at the expense of eclogite-facies felsic and basic rocks. They suggest that the minimum amount of fluid interacting with the wall-rocks was 0.1-0.5 wt%. In our samples, a retrograde hydration is recorded in significantly only in one sample (FG12157), for which P-T modelling indicates a second fluid influx at 1.4 GPa and 650°C (Rim2). In addition, several of our samples do show minor amounts of hydration during retrograde greenschist facies, but that effect is local and minor (<5% retrogression in most samples). A strong greenschist overprint (replacing 50-90% of the eclogite parageneses) is limited to the vicinity of the major tectonic contact between the IC and EC (Barmet Shear Zone; Giuntoli and Engi, 2016). By analogy we surmise that the hydration stage described by Konrad-Schmolke et al.

(2011) is a relatively late phenomenon occurring in a confined area during retrograde blueschist conditions, whereas the main hydration of the Internal Complex in the region of Aosta Valley occurred during the prograde P-T trajectory, at eclogite facies conditions, as described in this study.

The timing of fluid infiltration is reflected by Alpine allanite and zircon ages (Regis et al., 2014;Rubatto et al., 2011;Giuntoli, 2016;Giuntoli et al., submitted) and reflects asynchronicity, with older ages (85-77 Ma) generally in the internal (SE) areas of the IC, and younger ages (72-55 Ma) towards external areas (NW).

Unlike in the Norwegian Caledonides, the relationships between deformation structures that acted as fluid pathways (e.g. Austrheim, 1987) is not clear in our samples. Eclogitization of pre-Alpine granulites and amphibolites in the IC seems to be more an effect of pervasive but disperse fluid infiltration, not of a channelized flow. Based on mesoscopic evidence in the IC, the total amount of accumulated strain in the entire complex is fairly high, which may account for the disperse fluid flow. At the microscale sample FG1249 may be considered an exception, since it shows tracks of more channelized fluid flow preserved in millimetric garnets.

In Norway, lithological heterogeneities do not seem to play a major role in the localization of deformation. As shown by detailed mapping, the Internal Complex of the Sesia Zone consists of a pile of tectonic sheets, a few kilometres in thickness (Giuntoli and Engi, 2016). These sheets show internal lithological heterogeneity, with micaschist, eclogites, minor para- and orthogneiss interlayered at scales from a few millimetres to about a hundred metres. The rheological contrasts among these different rock bodies might well have been where small-scale shear bands nucleated that were served as conduits for fluid infiltration (Oliver, 1996).

7 Conclusions

This study documents complexly zoned garnet in polyorogenic rocks that were extensively deformed and (re)hydrated during Alpine eclogite facies metamorphism. Garnet in pelitic schists commonly preserves a porphyroclastic core that reflects medium-pressure HT-metamorphism. These granulite facies conditions prevailed during the Permian and converted the sedimentary protoliths to mostly anhydrous assemblages, which are locally preserved in the area studied. However, in the sample suite reported here, pre-Alpine conditions are evident only in relic zircon and garnet cores. Both of these show brittle deformation textures of tectonic origin that reflect high strain rates at the onset of Alpine tectonics. In garnet, a network of micrometre-size fractures crosscut the core (and locally a first Alpine overgrowth), and these cracks were sealed by a new generation of garnet. Its composition is more calcic and corresponds to the Alpine HP-rims of garnet.

The interaction of percolating fluid with garnet repeatedly produced resorption features, such as lobate structures, peninsulas, or atoll garnet. Textures indicating limited resorption are less common. In rocks where these features are present, re-equilibration produced by intragranular diffusion is located in proximity to brittle fractures, which acted as fluid pathways. Re-equilibration of Mg, Fe and Mn due to diffusion enhanced by fluid occurred over distances of several hundred micrometres, while Ca re-equilibrated over a much smaller distance due to slower diffusion. The intensity of prograde

hydration and HP-overprinting, as reflected in the preserved garnet textures, varies among the samples analysed. The set as a whole indicates regional differences, notably the fluid-garnet interaction intensity appears to a decrease (from SE to NW) over a few kilometres within the Internal Complex of the Sesia Zone. In some areas of the same complex, other studies found a further phase of decompression-related (blueschist facies) hydration that appears to be related to a major shear zone.

5   In most external (NW) parts of the Sesia zone studied here, a later, strong greenschist overprint is dominant.

This study shows that compositional (X-ray) maps are a powerful tool to document detailed mineral textures, particularly in garnet. When combined with thermobarometric results, such images facilitate the analysis of local processes, acting at (sub)grain scale, such as local growth and resorption, which play a critical role in hydrating HT protoliths and converting them to eclogite facies assemblages.

10   Data availability

Original data underlying the material presented care available by contacting the authors.

Competing interests.

The authors declare that they have no conflict of interest.

Acknowledgements

15   We thank Martin Robyr for his help in performing EMPA. Discussions with him and Jörg Hermann have been particularly fruitful. This work was supported by the Swiss National Science Foundation (Project 200020-146175).

References

Ague, J. J., and Carlson, W. D.: Metamorphism as garnet sees it: the kinetics of nucleation and growth, equilibration, and diffusional relaxation, Elements, 9, 439-445, 2013.

Ague, J. J., and Axler, J. A.: Interface coupled dissolution-reprecipitation in garnet from subducted granulites and ultrahigh-pressure rocks revealed by phosphorous, sodium, and titanium zonation, Am. Mineral., 101, 1696-1699, 2016.

Angiboust, S., Agard, P., Yamato, P., and Raimbourg, H.: Eclogite breccias in a subducted ophiolite: A record of intermediate-depth earthquakes?, Geology, 40, 707-710, 2012.

Artini, E., and Melzi, G.: Ricerche petrografiche e geologiche sulla Valsesia, Tipografia Bernardoni di C. Rebeschini, 1900.

Atherton, M., and Edmunds, W.: An electron microprobe study of some zoned garnets from metamorphic rocks, Earth Planet. Sci. Lett., 1, 185-193, 1966.

Austrheim, H.: Eclogitization of lower crustal granulites by fluid migration through shear zones, Earth Planet. Sci. Lett., 81, 221-232, 10.1016/0012-821X(87)90158-0, 1987.

Austrheim, H.: The granulite-eclogite facies transition: A comparison of experimental work and a natural occurrence in the Bergen Arcs, western Norway, Lithos, 25, 163–169, http://dx.doi.org/10.1016/0024-4937(90)90012-P, 1990.

Austrheim, H., Erambert, M., and Boundy, T. M.: Garnets recording deep crustal earthquakes, Earth Planet. Sci. Lett., 139, 223-238, 1996.

Austrheim, H., Erambert, M., and Engvik, A. K.: Processing of crust in the root of the Caledonian continental collision zone: the role of eclogitization, Tectonophysics, 273, 129-153, 1997.

Austrheim, H., Dunkel, K. G., Plümper, O., Ildefonse, B., Liu, Y., and Jamtveit, B.: Fragmentation of wall rock garnets during deep crustal earthquakes, Science Advances, 3, e1602067, 2017.

Babist, J., Handy, M. R., Hammerschmidt, K., and Konrad-Schmolke, M.: Precollisional, multistage exhumation of subducted continental crust: The Sesia Zone, western Alps, Tectonics, 25, 10.1029/2005TC001927, 2006.

Bearth, P.: Die Ophiolite der Zone von Zermatt-Saas Fee, Beiträge zur Geologischen Karte der Schweiz, 132, 130, 1967.

Beltrando, M., Manatschal, G., Mohn, G., Dal Piaz, G. V., Brovarone, A. V., and Masini, E.: Recognizing remnants of magma-poor rifted margins in high-pressure orogenic belts: The Alpine case study, Earth-Science Reviews, 131, 88-115, 2014.

Bertolani, M.: La formazione basica "Ivrea-Verbano" e la sua posizione nel quadro geologico-petrografico della bassa Val Sesia e del Biellese, Periodico di Mineralogia, 28, 151-209, 1959.

Bucher, K., Fazis, Y., Capitani, C. D., and Grapes, R.: Blueschists, eclogites, and decompression assemblages of the Zermatt-Saas ophiolite: High-pressure metamorphism of subducted Tethys lithosphere, Am. Mineral., 90, 821-835, 2005.

Caddick, M. J., Konopásek, J., and Thompson, A. B.: Preservation of garnet growth zoning and the duration of prograde metamorphism, J. Petrol., 51, 2327-2347, 2010.

Carlson, R. W., and Gordon, C. L.: Effects of matrix grain size on the kinetics of intergranular diffusion, J. Metamorph. Geol., 22, 733-742, 2004.

Carlson, W. D.: Dana Lecture. Rates of Fe, Mg, Mn, and Ca diffusion in garnet, Am. Mineral., 91, 1-11, 2006.

Cartwright, I., and Barnicoat, A.: Petrology, geochronology, and tectonics of shear zones in the Zermatt–Saas and Combin zones of the Western Alps, J. Metamorph. Geol., 20, 263-281, 2002.

Castelli, D.: Eclogitic metamorphism in carbonate rocks: the example of impure marbles from the Sesia-Lanzo Zone, Italian Western Alps, J. metamorphic Geol., 9, 61-77, 1991.

Cheng, A., Nakamura, E., Kobayashi, K., and Zhou, Z.: Origin of atoll garnets in eclogites and implications for the redistribution of trace elements during slab exhumation in a continental subduction zone, Am. Mineral., 92, 1119-1129, 2007.

Compagnoni, R.: The Sesia-Lanzo Zone: high pressure-low temperature metamorphism in the Austroalpine continental margin, Rend. Soc. Ital. Mineral. Petrol., 33, 335-375, 1977.

Compagnoni, R., Dal Piaz, G., Hunziker, J., Gosso, G., Lombardo, B., and Williams, P.: The Sesia-Lanzo Zone, a slice of continental crust with Alpine high pressure-low temperature assemblages in the Western Italian Alps, Rend. Soc. Ital. Mineral. Petrol, 33, 281-334, 1977.

Compagnoni, R., and Hirajima, T.: Superzoned garnets in the coesite-bearing Brossasco-Isasca Unit, Dora-Maira massif, Western Alps, and the origin of the whiteschists, Lithos, 57, 219-236, 2001.

Cooper, A.: Progressive metamorphism of metabasic rocks from the Haast Schist Group of southern New Zealand, J. Petrol., 13, 457-492, 1972.

Cruz, M. D. R.: Origin of atoll garnet in schists from the Alpujárride Complex (Central zone of the Betic Cordillera, Spain): Implications on the PT evolution, Mineral. Petrol., 101, 245-261, 2011.

Dal Piaz, G. V., Gosso, G., and Martinotti, G.: La II Zona Diorito-Kinzigitica tra la Valle Sesia e la Valle d'Ayas (Alpi Occidentali), Memorie della Società Geologica Italiana, 11, 433–460, 1971.

Dal Piaz, G. V., and Ernst, W. G.: Areal geology and petrology of eclogites and associated metabasalts of the Piemonte ophiolite nappe, Breuil-St. Jaques area, Italian Western Alps, Tectonophysics, 51, 99-126, 1978.

Dal Piaz, G. V.: The Austroalpine-Piedmont nappe stack and the puzzle of the Alpine Tethys, Mem. Sci. Geol., 51, 155-176, 1999.

Dewey, J., Helman, M., Knott, S., Turco, E., and Hutton, D.: Kinematics of the western Mediterranean, Geological Society, London, Special Publications, 45, 265-283, 1989.

Engi, M., Giuntoli, F., Lanari, P., Burn, M., Kunz, B. E., and Bouvier, A.-S.: Brittle deformation and rehydration of lower continental crust during subduction trigger pervasive eclogite formation. Implications on continental recycling, Geochemistry, Geophysics, Geosystems (G^3), in preparation.

Erambert, M., and Austrheim, H.: The effect of fluid and deformation on zoning and inclusion patterns in poly-metamorphic garnets, Contrib. Mineral. Petrol., 115, 204-214, 1993.

Faryad, S., Klápová, H., and Nosál, L.: Mechanism of formation of atoll garnet during high-pressure metamorphism, Mineral. Mag., 74, 111-126, 2010.

Floess, D., and Baumgartner, L.: Formation of garnet clusters during polyphase metamorphism, Terra Nova, 25, 144-150, 2013.

Florence, F. P., and Spear, F. S.: Effects of diffusional modification of garnet growth zoning on PT path calculations, Contrib. Mineral. Petrol., 107, 487-500, 1991.

Ganguly, J.: Cation diffusion kinetics in aluminosilicate garnets and geological applications, Rev. Mineral. Geochem., 72, 559-601, 2010.

Giuntoli, F.: Assembly of continental fragments during subduction at HP: Metamorphic history of the cetral Sesia Zone (NW Alps), PhD thesis, University of Bern, Switzerland, 2016.

Giuntoli, F., and Engi, M.: Internal geometry of the central Sesia Zone (Aosta Valley, Italy): HP tectonic assembly of continental slices, Swiss J. Geosci., 109, 445-471, 2016.

Giuntoli, F., Lanari, P., Burn, M., Kunz, B. E., and Engi, M.: Deeply subducted continental fragments: II. Insight from petrochronology in the central Sesia Zone (Western Italian Alps), Solid Earth, submitted.

Gosso, G., Messiga, B., Rebay, G., and Spalla, M. I.: Interplay between deformation and metamorphism during eclogitization of amphibolites in the Sesia-Lanzo Zone of the Western Alps, Int. Geol. Rev., 52, 1193-1219, 2010.

Groppo, C., Beltrando, M., and Compagnoni, R.: The P–T path of the ultra-high pressure Lago di Cignana and adjoining high-pressure meta-ophiolitic units: insights into the evolution of the subducting Tethyan slab, J. Metamorph. Geol., 27, 207-231, 2009.

Hames, W., and Menard, T.: Fluid-assisted modification of garnet composition along rims, cracks, and mineral inclusion boundaries in samples of amphibolite facies schists, Am. Mineral., 78, 338-344, 1993.

Handy, M. R., Schmid, S. M., Bousquet, R., Kissling, E., and Bernoulli, D.: Reconciling plate-tectonic reconstructions of Alpine Tethys with the geological–geophysical record of spreading and subduction in the Alps, Earth-Science Reviews, 102, 121-158, 2010.

Homam, S. M.: Formation of atoll garnet in the Ardara Aureole, NW Ireland, Journal of Sciences Islamic Republic of Iran, 14, 247-258, 2003.

Konrad-Schmolke, M., Babist, J., Handy, M. R., and O'Brien, P. J.: The physico-chemical properties of a subducted slab from garnet zonation patterns (Sesia Zone, Western Alps), J. Petrol., 47, 2123-2148, 2006.

Konrad-Schmolke, M., O'Brien, P. J., and Zack, T.: Fluid migration above a subducted slab – Constraints on amount, pathways and major element mobility from partially overprinted eclogite-facies rocks (Sesia Zone, Western Alps), J. Petrol., 52, 457-486, 10.1093/petrology/egq087, 2011.

Konrad-Schmolke, M., and Halama, R.: Combined thermodynamic–geochemical modeling in metamorphic geology: Boron as tracer of fluid–rock interaction, Lithos, 208, 393-414, 2014.

Kretz, R.: Chemical study of garnet, biotite and hornblende from gneisses of S.W. Quebec, with emphases on distribution of elements in coexisting minerals, Journal of Geology, 67, 371-402, 10.1086/626594, 1959.

Kunz, B. E., Manzotti, P., von Niederhäusern, B., Engi, M., Darling, J. R., Giuntoli, F., and Lanari, P.: Permian high-temperature metamorphism in the Western Alps (NW Italy), Int. J. Earth Sci., 1-27, 10.1007/s00531-017-1485-6, 2017.

Lanari, P., Riel, N., Guillot, S., Vidal, O., Schwartz, S., Pêcher, A., and Hattori, K. H.: Deciphering high-pressure metamorphism in collisional context using microprobe mapping methods: Application to the Stak eclogitic massif (northwest Himalaya), Geology, 41, 111-114, 2013.

Lanari, P., Vidal, O., Lewin, E., Dubacq, B., De Andrade, V., and Schwartz, S.: XMapTools a Matlab©--based graphic user interface for microprobe quantified image processing, Computers and Geosciences, 10.1016/j.cageo.2013.08.010, 2014.

Lanari, P., Giuntoli, F., Loury, C., Burn, M., and Engi, M.: An inverse modeling approach to obtain P-T conditions of metamorphic stages involving garnet growth and resorption, Eur. J. Mineral., 29, 181-199, 10.1127/ejm/2017/0029-2597, 2017.

Lardeaux, J. M., and Spalla, M. I.: From granulites to eclogites in the Sesia zone (Italian Western Alps): a record of the opening and closure of the Piedmont ocean, J. metamorphic Geol., 9, 35-59, 1991.

Manzotti, P., Ballevre, M., Zucali, M., Robyr, M., and Engi, M.: The tectonometamorphic evolution of the Sesia–Dent Blanche nappes (internal Western Alps): review and synthesis, Swiss J. Geosci., 107, 309-336, 2014.

Martin, S., Tartarotti, P., and Dal Piaz, G.: The Mesozoic ophiolites of the Alps: A review, Bollettino di Geofisica teorica ed applicata, 36, 1994.

Martinotti, G.: Studio petrografico delle eclogiti della zona del Monte Mucrone e dei loro rapporti con i "micascisti eclogitici" incassanti, Unpublished Thesis, Universita Torino, 1970.

Negro, F., Bousquet, R., Vils, F., Pellet, C.-M., and Hänggi-Schaub, J.: Thermal structure and metamorphic evolution of the Piemont-Ligurian metasediments in the northern Western Alps, Swiss J. Geosci., 106, 63-78, 2013.

O'Brien, P. J.: Garnet zoning and reaction textures in overprinted eclogites, Bohemian Massif, European Variscides: a record of their thermal history during exhumation, Lithos, 41, 119-133, 1997.

Oliver, N.: Review and classification of structural controls on fluid flow during regional metamorphism, J. Metamorph. Geol., 14, 477-492, 1996.

Ortolano, G., Visalli, R., Cirrincione, R., and Rebay, G.: PT-path reconstruction via unraveling of peculiar zoning pattern in atoll shaped garnets via image assisted analysis: an example from the Santa Lucia del Mela garnet micaschists (northeastern Sicily-Italy), Periodico di Mineralogia, 83, 257-297, 2014.

Pognante, U.: Lawsonite, blueschist and eclogite formation in the southern Sesia zone (Western Alps, Italy), Eur. J. Mineral., 1, 89–104, 1989.

Putnis, A.: Mineral replacement reactions: from macroscopic observations to microscopic mechanisms, Mineral. Mag., 66, 689-708, 2002.

Putnis, A.: Mineral replacement reactions, Rev. Mineral. Geochem., 70, 87-124, 2009.

Putnis, A., and John, T.: Replacement processes in the Earth's crust, Elements, 6, 159-164, 2010.

Putnis, A.: Transient porosity resulting from fluid–mineral interaction and its consequences, Rev. Mineral. Geochem., 80, 1-23, 2015.

Raimbourg, H., Goffé, B., and Jolivet, L.: Garnet reequilibration and growth in the eclogite facies and geodynamical evolution near peak metamorphic conditions, Contrib. Mineral. Petrol., 153, 1-28, 2007.

Rebay, G., and Spalla, M. I.: Emplacement at granulite facies conditions of the Sesia–Lanzo metagabbros: an early record of Permian riftig?, Lithos, 58, 85–104, 2001.

Rebay, G., Spalla, M. I., and Zanoni, D.: Interaction of deformation and metamorphism during subduction and exhumation of hydrated oceanic mantle: Insights from the Western Alps, J. Metamorph. Geol., 30, 687-702, 10.1111/j.1525-1314.2012.00990.x, 2012.

Regis, D., Rubatto, D., Darling, J., Cenki-Tok, B., Zucali, M., and Engi, M.: Multiple metamorphic stages within an eclogite-facies terrane (Sesia Zone, Western Alps) revealed by Th-U-Pb petrochronology, J. Petrol., 55, 1429-1456, 10.1093/petrology/egu029, 2014.

Robyr, M., Darbellay, B., and Baumgartner, L. P.: Matrix-dependent garnet growth in polymetamorphic rocks of the Sesia zone, Italian Alps, J. Metamorph. Geol., 32, 3-24, 2014.

Rosenbaum, G., Lister, G. S., and Duboz, C.: Relative motions of Africa, Iberia and Europe during Alpine orogeny, Tectonophysics, 359, 117-129, 2002.

Rubatto, D., Regis, D., Hermann, J., Boston, K., Engi, M., Beltrando, M., and McAlpine, S.: Yo-Yo subduction recorded by accessory minerals (Sesia Zone, Western Alps) Nat. Geosci., 4, 338-342, 10.1038/ngeo1124, 2011.

Smellie, J.: Formation of atoll garnets from the aureole of the Ardara pluton, Co. Donegal, Ireland, Mineral. Mag., 39, 878-888, 1974.

Spear, F.: On the interpretation of peak metamorphic temperatures in light of garnet diffusion during cooling, J. Metamorph. Geol., 9, 379-388, 1991.

Spear, F. S., Selverstone, J., Hickmott, D., Crowley, P., and Hodges, K.: PT paths from garnet zoning: A new technique for deciphering tectonic processes in crystalline terranes, Geology, 12, 87-90, 1984.

Spiess, R., Peruzzo, L., Prior, D., and Wheeler, J.: Development of garnet porphyroblasts by multiple nucleation, coalescence and boundary misorientation-driven rotations, J. Metamorph. Geol., 19, 269-290, 2001.

Trepmann, C. A., and Stöckhert, B.: Cataclastic deformation of garnet: a record of synseismic loading and postseismic creep, J. Struct. Geol., 24, 1845-1856, 2002.

Ushakova, E., and Usova, L.: Atoll garnets in the contact aureole of an area of southeastern Tuva, Geologia i Geofizika, 31, 50-59, 1990.

Venturini, G., Martinotti, G., Armando, G., Barbero, M., and Hunziker, J. C.: The Central Sesia–Lanzo Zone (Western Italian Alps): new field observations and lithostratigraphic subdivisions, Schweiz. Mineral. Petrogr. Mitt., 74, 111-121, 1994.

Wassmann, S., and Stöckhert, B.: Low stress deformation of garnet by incongruent dissolution precipitation creep, J. Struct. Geol., 46, 200-219, 2013.

Whitney, D. L., and Evans, B. W.: Abbreviations for names of rock-forming minerals, Am. Mineral., 95, 185, 2010.

Yardley, B. W. D.: An empirical study of diffusion in garnet, Am. Mineral., 62, 793-800, 1977.

Zingg, A.: The Ivrea and Strona Ceneri Zones (Southern Alps, Ticino and Northern Italy): A review., Schweiz. Mineral. Petrogr. Mitt., 63, 361-392, 1983.

Zucali, M., Spalla, M. I., and Gosso, G.: Strain partitioning and fabric evolution as a correlation tool: the example of the Eclogitic Micaschists Complex in the Sesia–Lanzo Zone (Monte Mucrone–Monte Mars, Western Alps, Italy), Schweiz. Mineral. Petrogr. Mitt., 82, 429–454, 2002.

Zucali, M., and Spalla, M. I.: Prograde lawsonite during the flow of continental crust in the Alpine subduction: Strain vs. metamorphism partitioning, a field-analysis approach to infer tectonometamorphic evolutions (Sesia-Lanzo Zone, Western Italian Alps), J. Struct. Geol., 33, 381-398, 2011.
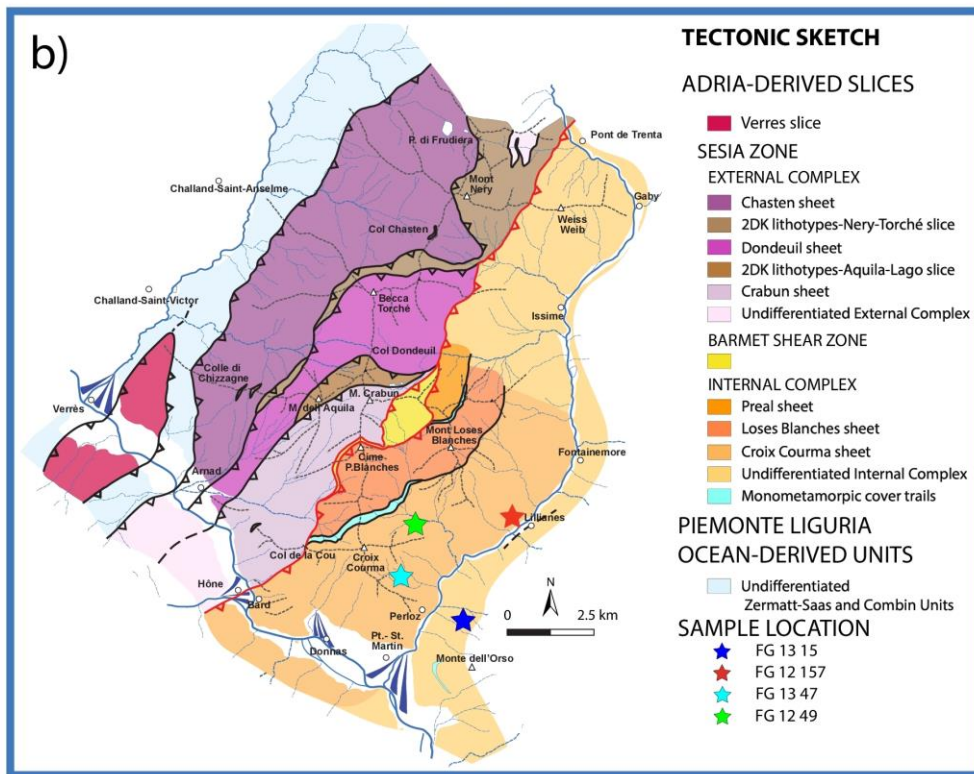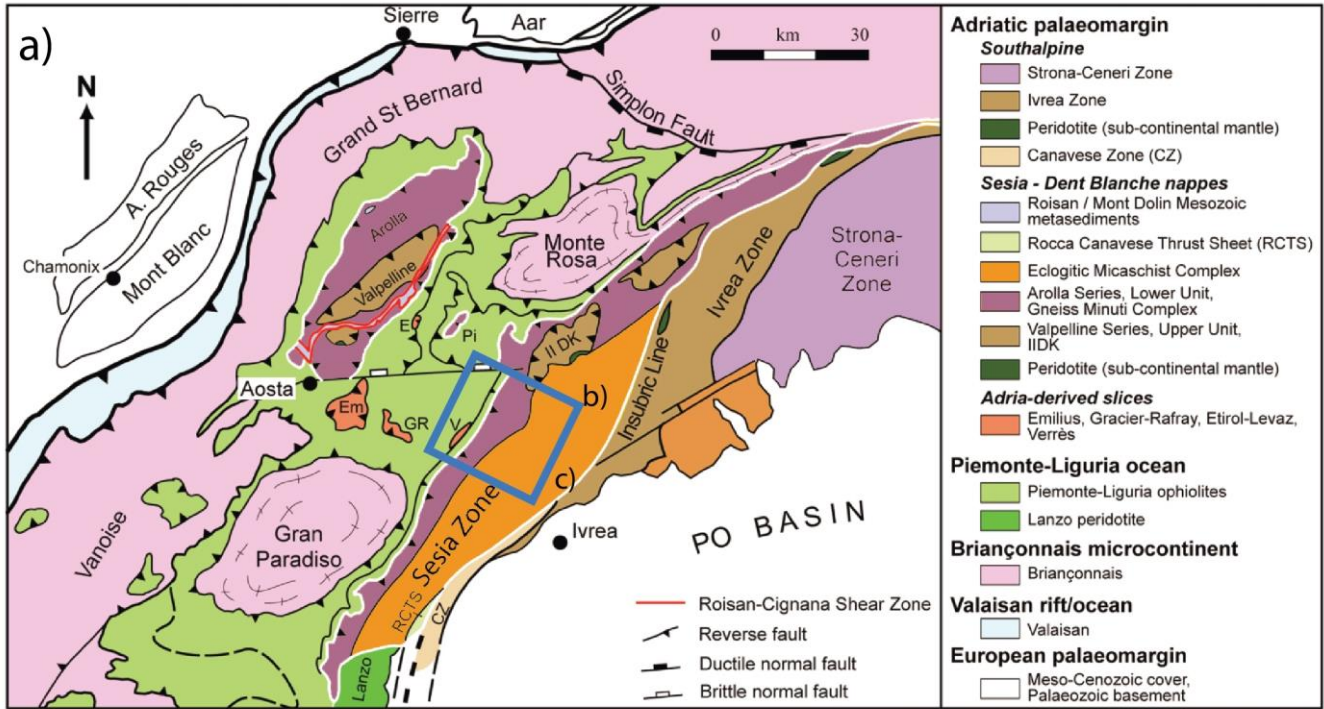
Figure 1: (a) Simplified tectonic map of the Western Alps (modified from Manzotti et al. (2014), location of study area. (b) Tectonic sketch of study area with sample locations (modified from Giuntoli and Engi, 2016).
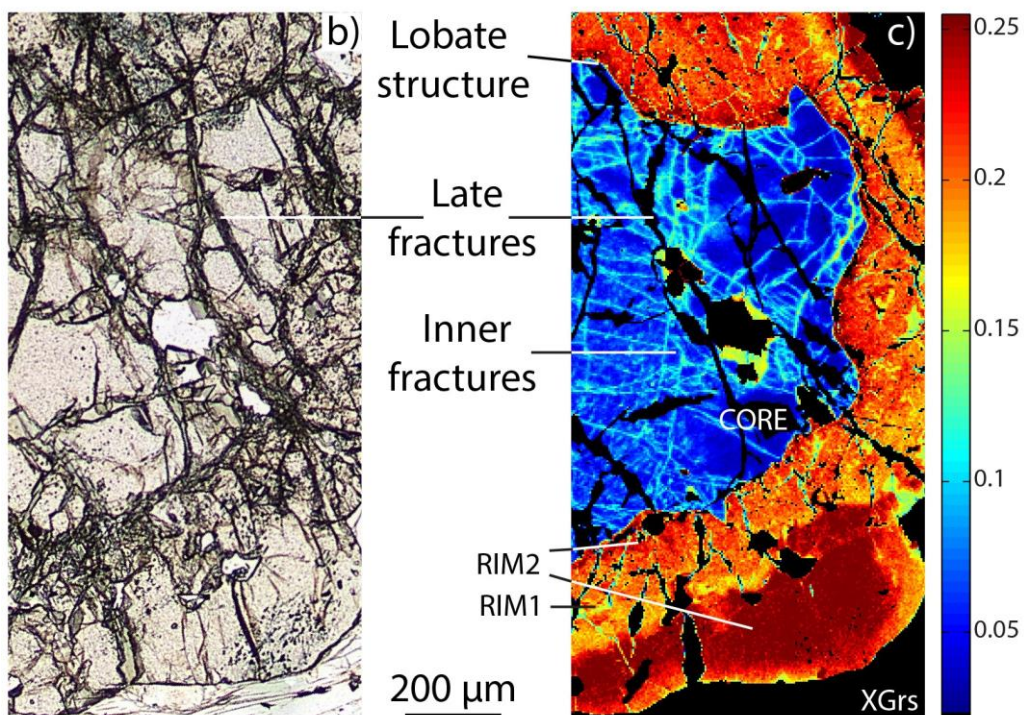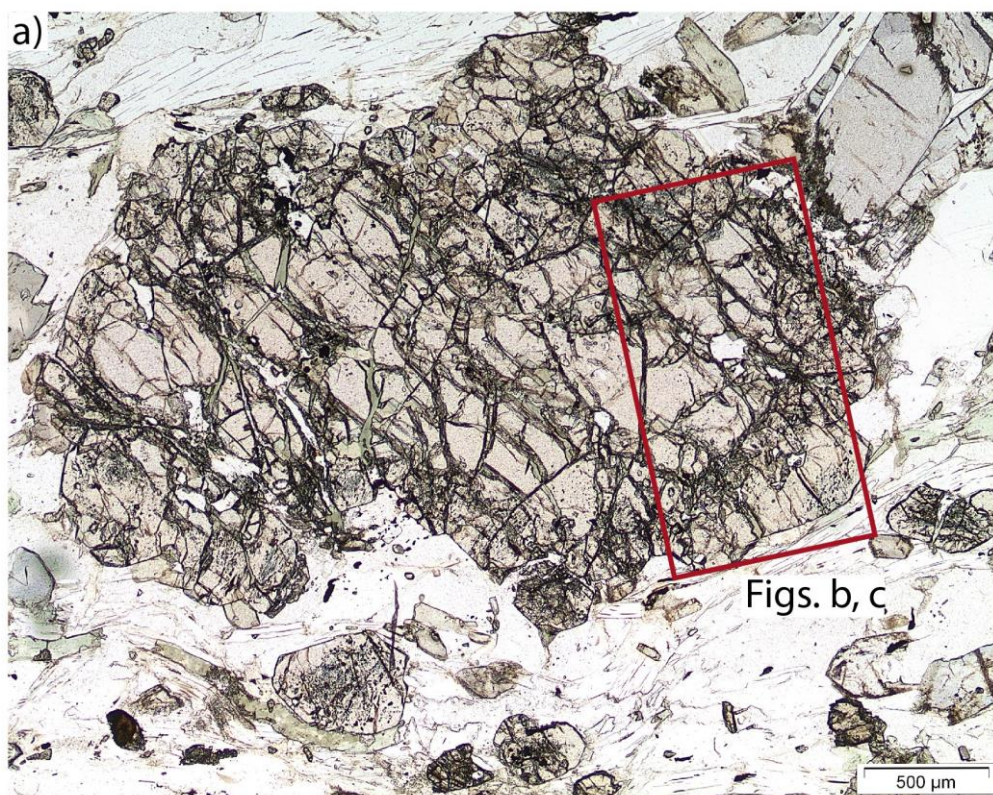
Figure 2: Garnet porphyrocryst in FG12157, (a) and (b): Optical microphoto, plane polarized light. (a): Clear lobate core, inner rim dark, speckled with inclusions (mostly rutile, up to 20 µm long), outer rim more clear with only minor inclusions. (b) Enlargement shows late fractures (dark) containing chlorite. c Grossular X-ray map; blue Ca-poor core reveals numerous micrometre-size fractures sealed by more calcic garnet; sparse late fractures (black) in core and rims. Compare to complete maps in Figs. 3b, 5.
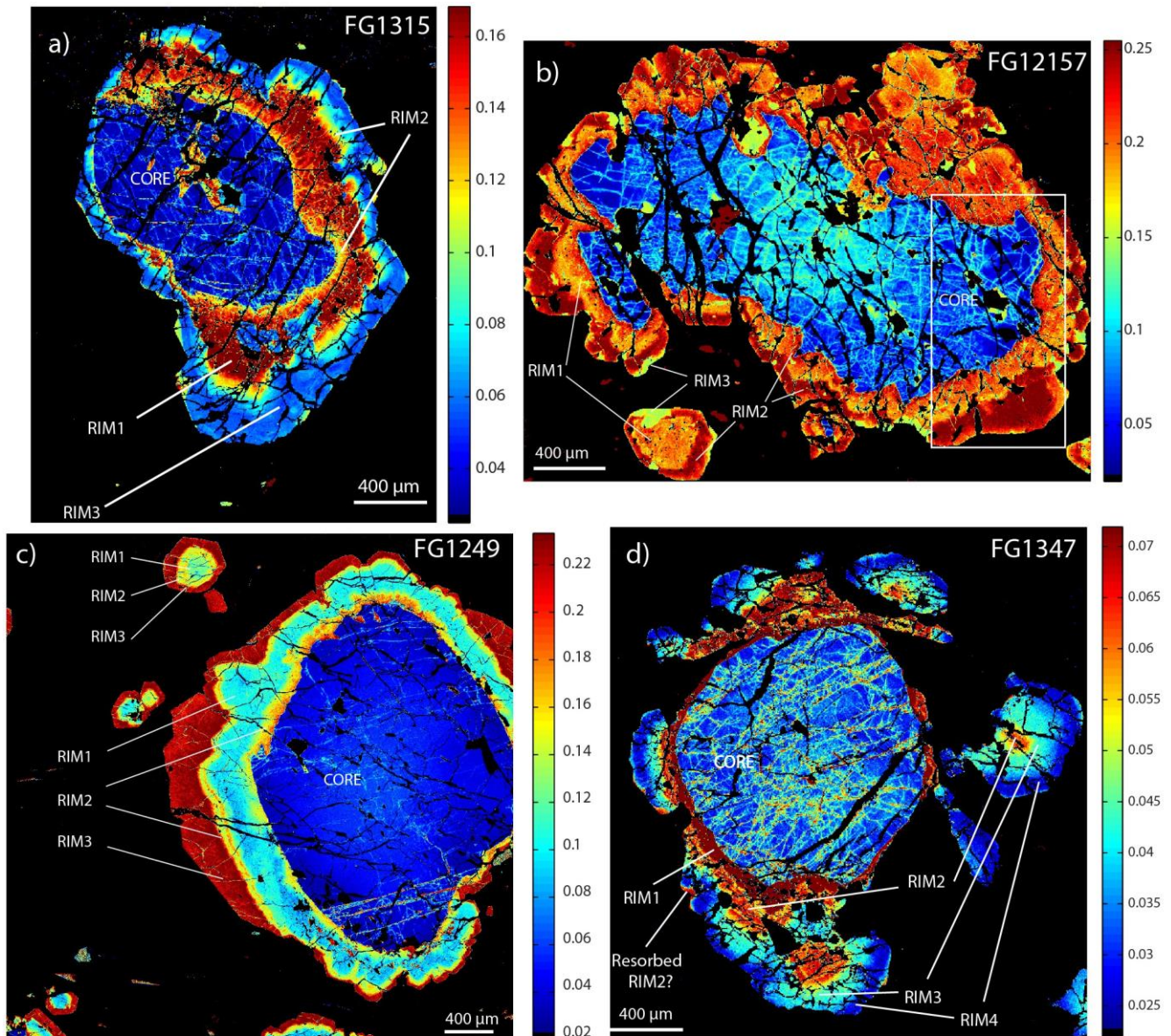
Figure 3: Growth zones visible in standardized X-ray maps for the grossular end-member. The foliation in all photos is horizontal. Note that a fractured core poor in X_{Grs} is present in all samples and always rimmed by several garnet

growth zones. In FG1315 (a) and FG12157 (b) textures indicating resorption include lobate edges and peninsulas (the white rectangle indicates the location of Figs. 2b, c). In FG1249 (c) resorption is inferred from the growth of Rim2 both inside and outside Rim1. In FG1347 (d) resorption is not so evident, but rims vary in thickness in each generation of overgrowths.
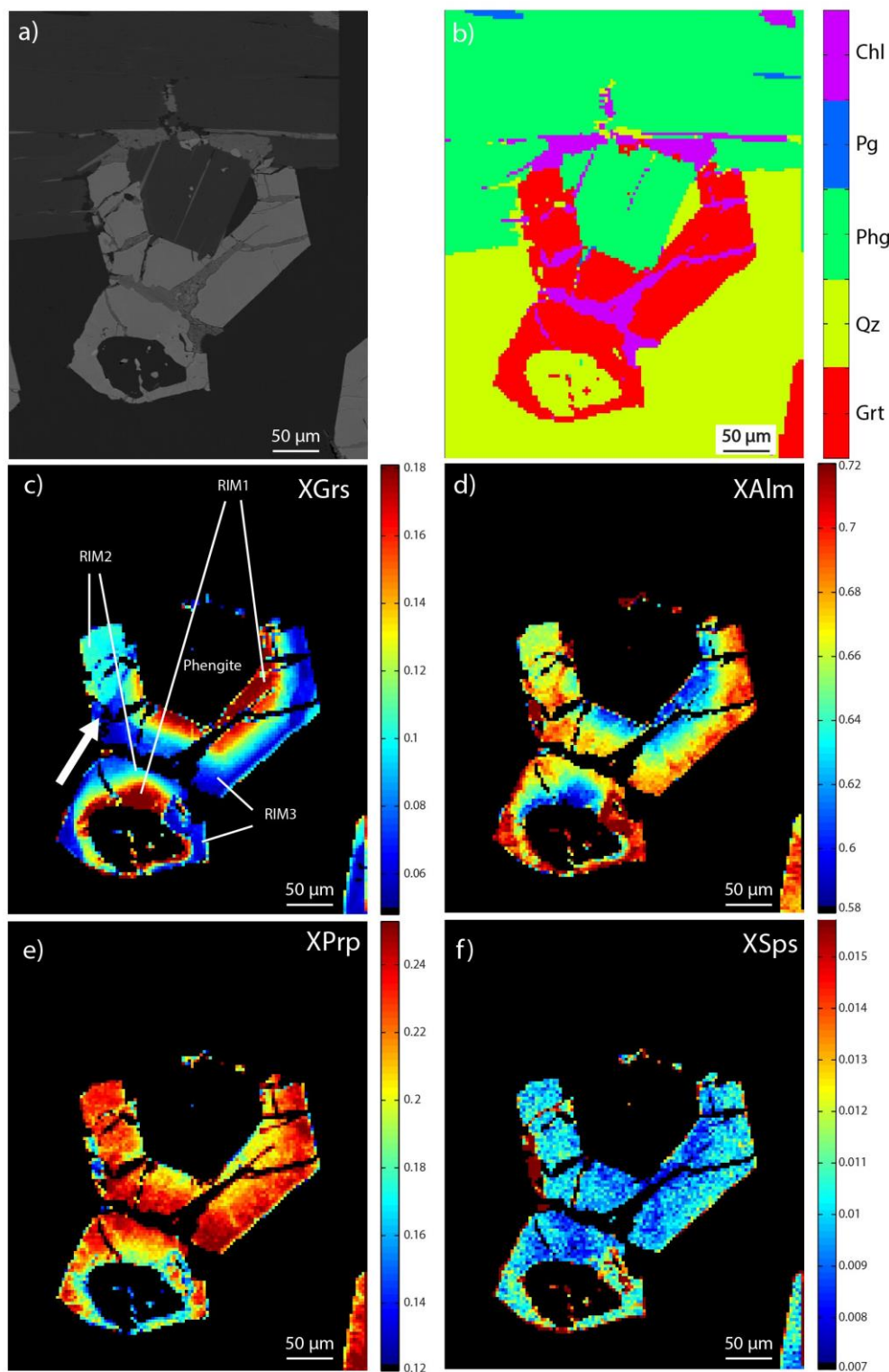
Figure 4: Small atoll garnet (ø ~100 μm) in sample FG1315. (a) BSE picture. (b) Mineral phases (determined from X-ray maps). Note inclusions of quartz and phengite in the atoll core; fractures dissecting garnet are filled by chlorite. Garnet occurs at the contact of quartz- and phengite-rich bands that define the main foliation. (c) Standardized X-ray map for the X_{Grs} end-member. Note the analogous zoning pattern as for large garnet (Fig. S5), with same X_{Grs} contents and a Rim3 peninsula extending into the resorbed rims (arrow). (d), (e), (f) Standardized X ray maps for X_{Alm}, X_{Prp}, and X_{Sps} respectively.
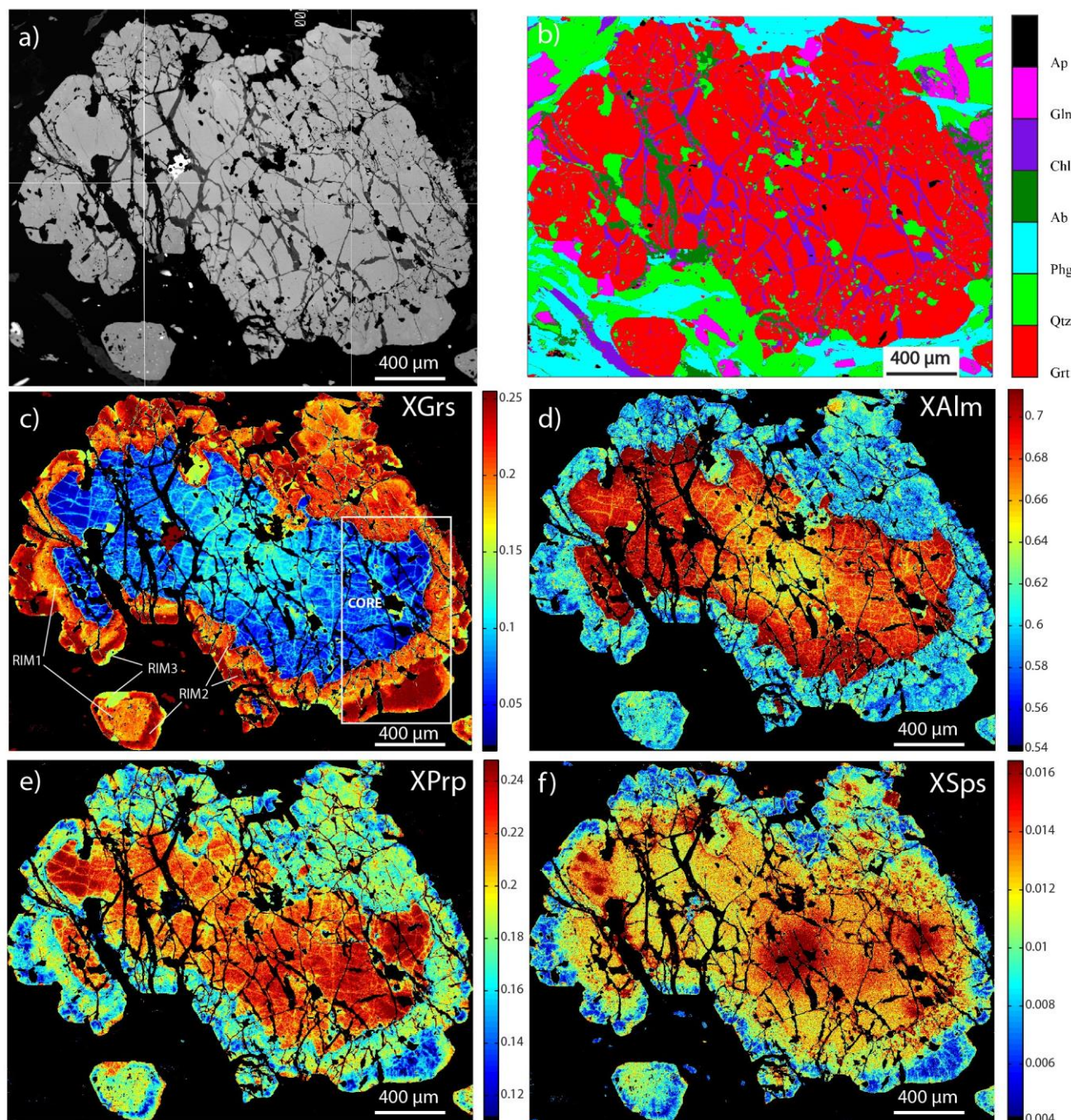
Figure 5: Large garnet (ø ~2-3 mm) in sample FG12157. (a) BSE picture with a bright porphyroclastic core and a darker rim. (b) Mineral phases (based on X-ray maps). Quartz inclusions are present in several garnet growth zones, but locally mark the core-Rim1 boundary; note that fractures (filled by chlorite and albite) dissect the entire garnet

grain. Glaucophane and phengite seem to be intergrown with garnet Rim2. c Standardized X-ray map for X_{Grs} end-member (the white rectangle indicates the location of Figs. 2b, (c). Note the lobate edges along the core and the fracture network within the core that is sealed by garnet higher in X_{Grs}. Zoning patterns in small garnet crystals are similar. (d), (e) Standardized X-ray maps for X_{Alm} and X_{Prp} display zoning inside the core. f Standardized X-ray map for X_{Sps}. The image appears fuzzy because Mn-contents are low. Note the areas with higher X_{Sps} in the core.
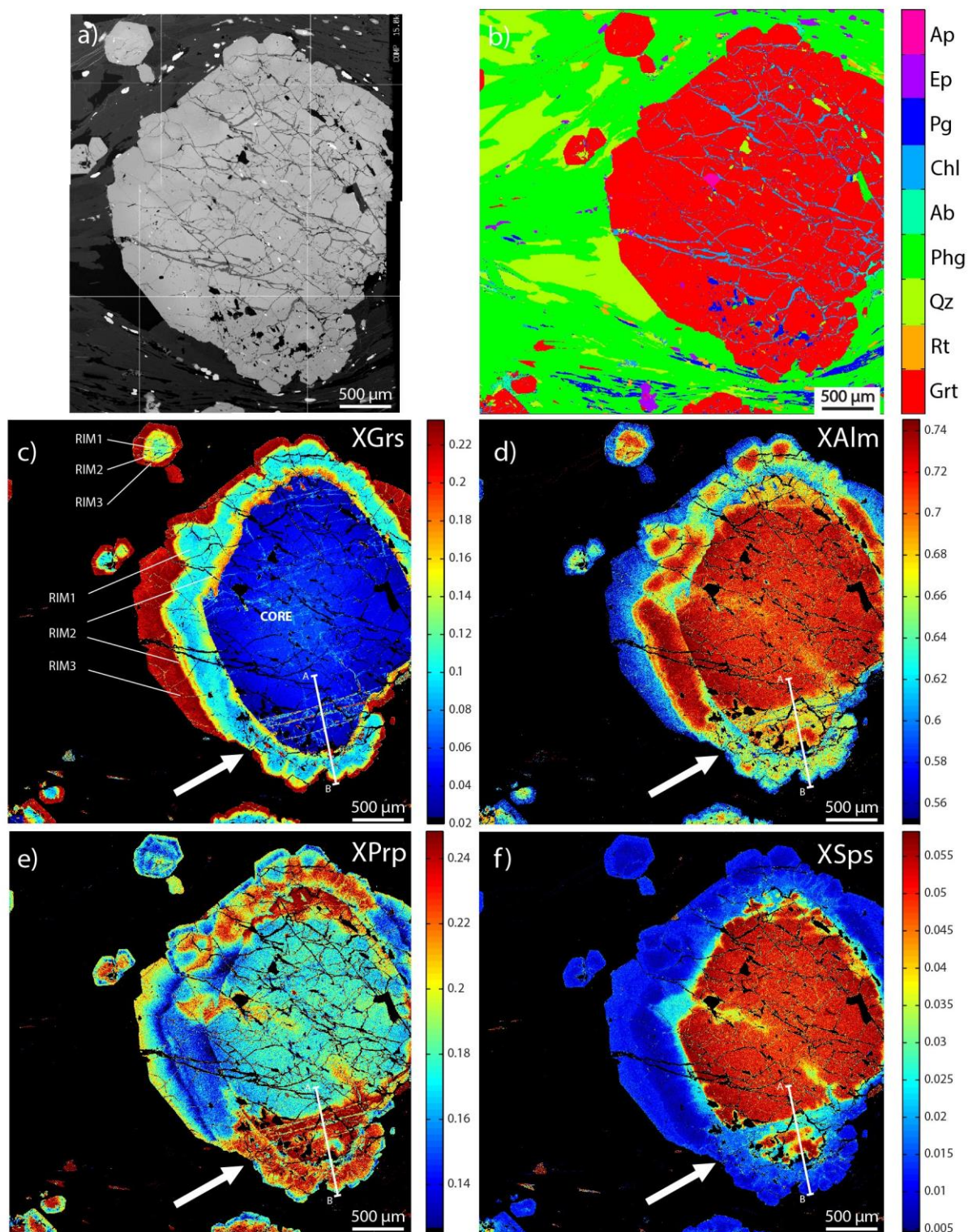
Figure 6: Large garnet (ø ~3 mm) in sample FG1249. (a) BSE picture shows bright porphyroclastic core and darker rim. (b) Mineral phases (based on X-ray maps). Quartz is included inside the core and at the core-rim boundary, paragonite inclusions are abundant in correspondence of the major fractures sealed by higher grossular garnet. Late fractures that dissect all the garnet are filled by chlorite and albite. (c) X_{Grs} map. Major fractures are sealed by higher grossular garnet. Smaller garnet grains have no core but rims showing the same zoning. (d), (e) and (f) X_{Alm}, X_{Prp} and X_{Sps} maps, respectively, highlighting beginning re-equilibration in the core and Rim1 near the major fractures (arrows). Incipient re-equilibration is also visible in X_{Prp} along the core-Rim1 boundary. Mn was remobilized and contributed to the growth of Rim2 and Rim3. Relics of the pristine core are preserved as islands inside re-equilibrated garnet Rim 2 and Rim3 (bottom part of figure). Note location of AB profile shown in Fig. 7.
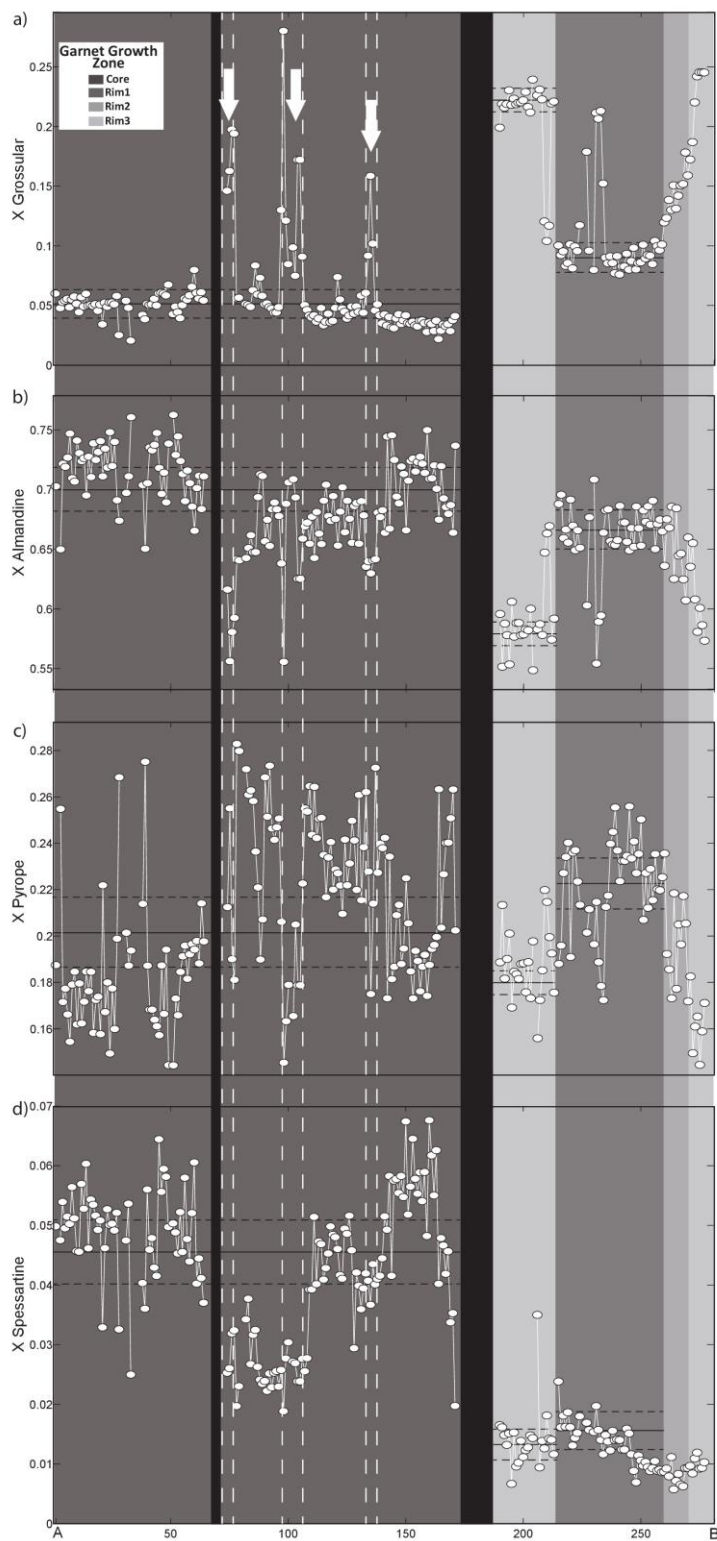
Figure 7: Garnet end-member proportions along 300 μm profile (trace shown in Fig. 6) in sample FG1249. Note different mole fraction scales. Late chlorite fractures are highlighted by black bands. The fractures in the core, sealed by a garnet with different composition, are indicated by white arrows. Mean compositions are represented by black solid lines with the standard deviation (1σ) represented by the dashed black lines. (a) Grossular. (b) Almandine. (c) Pyrope. (d) Spessartine. The distinction of each garnet growth zone is based on its grossular content with the aim of helping the comparison.
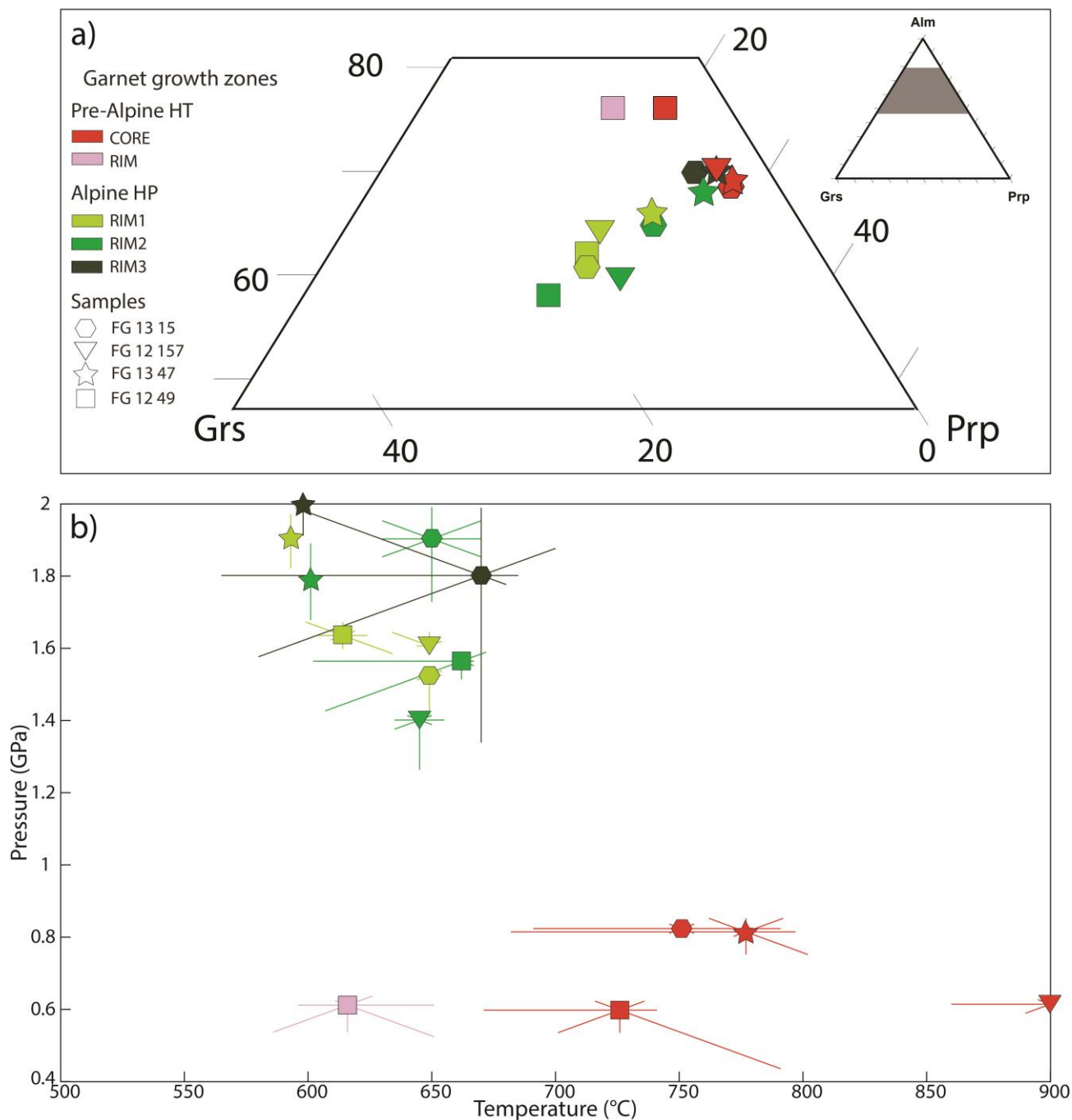
Figure 8: (a) Molar proportions of garnet in growth zones from the four micaschists. (b) P-T diagram with a summary of the modelled conditions for each garnet growth zone. Note major difference in P-T conditions from the pre-Alpine to the Alpine generations. The effect of uncertainties in each set of isopleths is shown around the P-T

model of each growth zone (dataset from Lanari et al., 2017 and Giuntoli, 2016) For sample FG1249 the pre-Alpine rim (pink) corresponds to Rim1, Rim 1 to Rim 2 and Rim 2 to Rim 3 in the text.
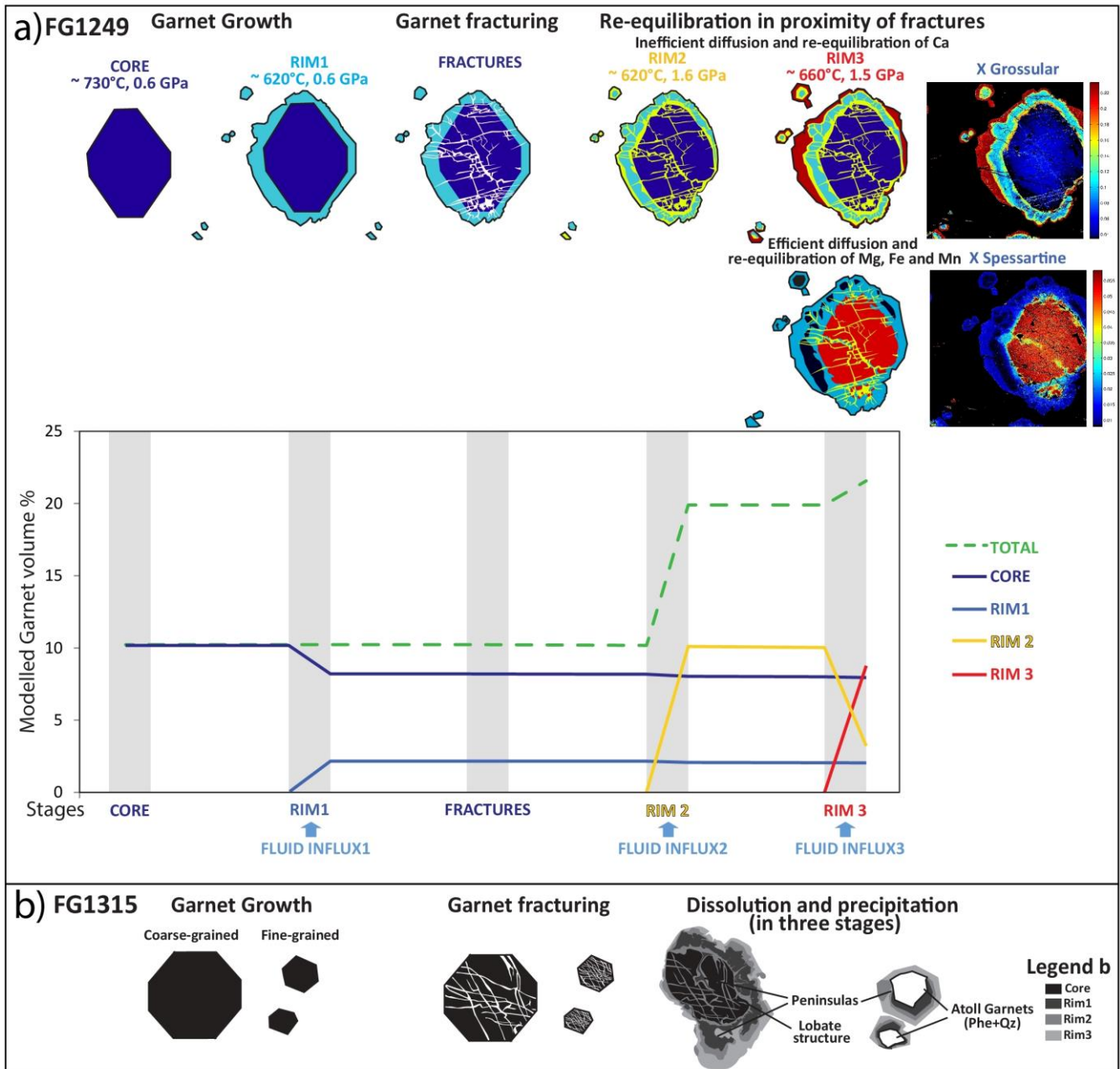
Figure 9: (a) Sketch illustrating the inferred chronology of sample FG1249, from textural observations and thermodynamic modelling. The preserved succession of stages in garnet evolution is shown along the abscissa, the

modelled garnet volume along the ordinate; values include the sum total due to growth and resorption. Note the difference in P-T conditions for the core and Rim1 (both pre-Alpine), relative to Rim2 and 3 (both Alpine); the three fluid pulses are related to Rim1, 2 and 3 growths. After the growth of core and Rim1, a fracture network developed, indicating high strain rates. These fractures acted as fluid channels and in their proximity garnet core and Rim1 got

5   effectively re-equilibrated due to diffusion of Mg, Fe and Mn, whereas Ca remained more immobile. (b) Sketch illustrating the sequence of processes inferred from garnet textures in samples FG1315. Fracture networks are visible in all the garnet core grain sizes. Subsequent stages of fluid influxes caused dissolution of the previous garnet generation/s and precipitation of new garnet, producing peninsulas, lobate structures and atoll structures in smaller garnet grains.

Sample	Minerals	Garnet growth zones	Sample locations
FG1315	Qz, Ph, Pg, Grt, Ep, Chl, Ab, Rt, Gr, Zrn	Pre-Alpine core + 3 Alpine rims. Note: atoll garnet	Rechantier, X= 408514, Y= 5051580
FG12157	Qz, Ph, Grt, Gln, Ep, Chl, Ab, Rt, Zrn, Ilm, Gr	Pre-Alpine core + 2 Alpine rims	Lillianes, X= 409683, Y= 5054033
FG1249	Qz, Ph, Pg, Grt, Ep, Chl, Ab, Rt, Gln, Zrn	Pre-Alpine core and Rim1 + 2 Alpine rims	Faye, X= 406637, Y= 5053931
FG1347	Qz, Ph, Pg, Cld, Grt, Ep, Chl, Rt, Zrn	Pre-Alpine core + 4 Alpine rims	Liévanere, X= 406318, Y= 5052474

Table1: Micaschists analysed (all from the Lys Valley). Mineral abbreviations from Whitney and Evans (2010). Coordinates refer to ED 1950 UTM Zone 32N.

Sample	FG1315				FG12157			FG1249				FG1347				
Garnet	CORE	RIM 1	RIM 2	RIM 3	CORE	RIM 1	RIM 2	CORE	RIM 1	RIM 2	RIM 3	CORE	RIM 1	RIM 2	RIM 3	RIM 4
Average composition (wt%)																
SiO_2	37.70	37.96	37.81	37.44	38.17	38.43	38.74	36.91	36.62	37.80	37.98	37.75	37.88	38.18	37.75	37.33
TiO_2	0.01	0.01	0.01	0.01	0.07	0.07	0.17	0.05	0.16	0.27	0.04	0.02	0.02	0.02	0.03	0.03
Al_2O_3	21.27	21.44	21.46	21.32	21.07	21.20	21.24	20.83	21.36	21.18	21.77	21.25	21.28	21.09	21.21	21.33
FeO	31.46	27.94	30.03	32.07	31.23	29.05	26.83	33.06	34.23	28.79	27.12	31.30	30.19	30.82	31.96	32.07
MnO	0.61	0.41	0.42	0.31	1.00	0.57	0.56	2.31	0.37	0.66	0.56	0.92	0.37	0.39	0.35	0.32
MgO	7.19	5.33	6.18	6.30	6.41	5.08	4.22	4.65	3.86	5.18	4.86	7.05	5.76	6.60	6.62	7.30
CaO	1.31	6.72	4.17	2.08	1.38	5.59	8.39	1.77	3.27	6.35	8.38	1.14	3.96	2.13	1.49	0.96
Cr_2O_3	0.00	0.00	0.00	0.00	0.04	0.04	0.04	0.03	0.04	0.03	0.03	0.00	0.00	0.00	0.00	0.00
Total	99.56	99.81	100.08	99.52	99.37	100.03	100.18	99.62	99.90	100.27	100.73	99.41	99.47	99.24	99.41	99.33
Formulae based on 12 oxygens																
Si	2.965	2.974	2.958	2.957	3.021	3.019	3.035	2.954	2.926	2.960	2.948	2.976	2.990	3.016	2.982	2.943
Ti	0.001	0.001	0.001	0.001	0.004	0.004	0.010	0.003	0.010	0.016	0.002	0.001	0.001	0.001	0.002	0.002
Al	1.972	1.980	1.979	1.985	1.965	1.963	1.961	1.965	2.011	1.955	1.991	1.974	1.979	1.964	1.975	1.981
Fe	2.069	1.831	1.965	2.119	2.067	1.908	1.758	2.213	2.287	1.885	1.760	2.064	1.992	2.035	2.111	2.114
Mn	0.041	0.027	0.028	0.021	0.067	0.038	0.037	0.157	0.025	0.044	0.037	0.061	0.025	0.026	0.023	0.022
Mg	0.843	0.623	0.720	0.741	0.756	0.595	0.493	0.555	0.459	0.605	0.563	0.828	0.677	0.777	0.780	0.858
Ca	0.110	0.564	0.350	0.176	0.117	0.470	0.704	0.152	0.280	0.533	0.697	0.096	0.335	0.180	0.126	0.081
$\sum$ cations	8.001	8.000	8.000	8.000	7.997	7.998	7.997	7.998	7.998	7.998	7.998	8.000	7.999	7.999	7.999	8.000
Molecular proportions of garnet end members																
Alm	0.676	0.601	0.641	0.693	0.687	0.634	0.588	0.719	0.750	0.615	0.576	0.677	0.658	0.674	0.694	0.688
Prp	0.275	0.204	0.236	0.242	0.252	0.198	0.165	0.180	0.150	0.197	0.184	0.272	0.224	0.257	0.256	0.279
Grs	0.036	0.186	0.114	0.058	0.039	0.156	0.235	0.050	0.092	0.174	0.228	0.031	0.111	0.060	0.042	0.026
Sps	0.013	0.009	0.009	0.007	0.022	0.013	0.012	0.051	0.008	0.014	0.012	0.020	0.008	0.009	0.008	0.007

Table2: Representative analyses of garnet growth zones